

1 **New Evidence for millennial-scale**
2 **interactions between Hg cycling and**
3 **hydroclimate from Lake Bosumtwi,**
4 **Ghana**

5 Alice R. Paine^{1,2*}, Joost Frieling¹, Timothy M. Shanahan², Tamsin A. Mather¹, Nicholas
6 McKay³, Stuart A. Robinson¹, David M. Pyle¹, Isabel M. Fendley¹, Ruth Kiely⁴, William D.
7 Gosling⁴

8 ¹Department of Earth Sciences, University of Oxford, UK, OX1 3AN

9 ^{2*}[Department of Environmental Sciences, University of Basel, Bernoullistrasse 32, CH-4056 Basel, Switzerland](#)

10 ³Department of Earth and Planetary Sciences, University of Texas at Austin, Texas, USA

11 ⁴School of Earth and Sustainability, Northern Arizona University, Flagstaff, Arizona, USA

12 ⁵Institute for Biodiversity & Ecosystem Dynamics, University of Amsterdam, Amsterdam, Netherlands

13 **Corresponding Author:** alice.paine@unibas.ch

14 ** current affiliation: Corresponding Author: alice.paine@earth.ox.ac.uk*

Formatted: Superscript

17 Changing hydrology impacts the biogeochemical cycling of elements such as mercury (Hg), whose
18 transport and transformation in the environment appear linked to hydroclimate on diverse timescales.
19 Key questions remain about how these processes manifest over different timescales and their potential
20 environmental consequences. For example, millennial-scale Hg-hydroclimate interactions in the
21 terrestrial realm are poorly understood, as few sedimentary records have sufficient length and/or
22 resolution to record abrupt and long-lasting changes in Hg cycling, and the relative roles of depositional
23 processes on these changes. Here, we present a high-resolution sedimentary Hg record from tropical
24 Lake Bosumtwi (Ghana, West Africa) since ~96 ka. A coupled response is observed between Hg flux and
25 shifts in sediment composition, the latter reflecting changes in lake level. Specifically, we find that the
26 amplitude and frequency of Hg peaks increase as the lake level rises, suggesting that Hg burial was
27 enhanced in response to an insolation-driven increase in precipitation at ~73 ka. A more transient,
28 threefold increase in Hg concentration and accumulation rate is also recorded between ~13 and 4 ka,
29 coinciding with a period of distinctly higher rainfall across North Africa known as the African Humid
30 Period. Two mechanisms, likely working in tandem, could explain this correspondence: (1) an increase in
31 wet deposition of Hg by precipitation and (2) efficient sequestration of organic-hosted Hg. Taken
32 together, our results reaffirm that changes in hydroclimate, directly and/or indirectly, can be linked to
33 millennial-scale changes in tropical Hg cycling, and that these signals can be recorded in lake
34 sediments.

35 **KEYWORDS:** [lacustrine, geochemistry, sediment, sapropel, organic, Africa](#)

36
37 **1. Introduction**

Mercury (Hg) is a volatile and toxic metal released into the atmosphere as a result of natural processes (e.g., volcanism, geothermal activity, weathering; Edwards et al., 2021; Selin, 2009) and, more recently, human activities (e.g., industrial activities, mining, coal burning; Amos et al., 2015). Approximately 95 % of atmospheric Hg exists in gaseous elemental form (Hg^0). An atmospheric lifetime of up to 2 years permits its transport over long distances prior to removal by wet or dry deposition, and following oxidation and aerosol scavenging (Lyman et al., 2020). Once free gaseous (Hg^0) and/or oxidised (Hg^{II}) Hg has been deposited into the terrestrial environment, two sets of reactions become particularly important: (1) oxidation-reduction, and (2) methylation-demethylation (Branfireun et al., 2020). The reduction of Hg^{II} to Hg^0 can result in release back into the atmosphere. Hg^{II} can also be bound to organic matter (OM) or sulphides, and thus be sequestered and accumulated in sediments (Åkerblom et al., 2013; Hsu-Kim et al., 2013; Mason et al., 2000). Accumulation of Hg in the terrestrial environment is therefore a function of the balance between Hg removal from and re-emission to the atmosphere, and governed by the rate and intensity of different thermal, photo, and biogenic reactions (Bishop et al., 2020; Obrist et al., 2018).

The exchange of Hg between the terrestrial biosphere, hydrosphere, critical zone, and atmosphere are intrinsically coupled to climate. Changes in ecosystem Hg loading, overland transport, and methylation have all been directly linked to decadal-scale changes in global temperature and precipitation, and their associated shifts in terrestrial productivity, land-atmosphere exchange, and wildfire dynamics (Bishop et al., 2020; Li et al., 2020). However, studying the long-term natural Hg cycle presents several challenges. For example, the overwhelming increase in anthropogenic Hg fluxes in recent decades have substantially altered the environmental dynamics of this cycle, complicating assessment of how long-term climate change may alter its rate, intensity, and evolution (United Nations Environment Programme, 2018). Pre-industrial-age archives allow for clear comparison between natural and anthropogenic-driven changes in Hg cycling, and identification of which regions may be most vulnerable to the negative effects of these changes, and highlight the importance of understanding the long-term Hg cycle (e.g., Cooke et al., 2020; Segato et al., 2023).

1.1 Mercury cycling and hydroclimate.

The transport and transformation of Hg at the Earth's surface is **directly**-linked to the hydrological cycle (Bishop et al., 2020; Selin, 2009). Water plays a direct role in the efficiency of both Hg deposition and re-emission. For example, changes in precipitation **patterns-amount** can influence the proportion of Hg removed from the atmosphere by wet versus dry deposition, with higher precipitation amounts generally corresponding to enhanced Hg deposition at the surface (Amos et al., 2015; Guédron et al., 2018). Elevated Hg concentrations have been measured in equatorial ocean surface waters corresponding to inter-annual peaks in precipitation, with general circulation model simulations suggesting that these are likely due to higher net Hg flux by wet deposition (Kuss et al., 2011; Soerensen et al., 2014; Sprovieri et al., 2010). Multi-year monitoring by the Global Mercury Observation System (GMOS) has similarly revealed distinct interannual differences in total wet

76 deposition of Hg, with the highest fluxes typically occurring in the wettest years (Leiva González et al.,
77 2022; Sprovieri et al., 2017). Precipitation also facilitates Hg transport in terrestrial watersheds, with
78 simultaneous increases in river discharge, surface runoff, and soil erosion during and after intense
79 storm events all enhancing hydrological 'connectivity' between surface environments and feeder
80 tributaries (Bishop et al., 2020). This enhances overland transport of Hg and other suspended
81 materials, and subsequently their delivery to lake and near-shore marine sediments (Liu et al., 2021;
82 Zaferani and Biester, 2021).

83 Water also plays an indirect role in drawdown and sequestration of Hg in aquatic environments.
84 Systems that are particularly sensitive to changes in water balance (e.g., terrestrial lakes) are most
85 likely to experience distinct, hydro-climate driven environmental changes that impact their internal Hg
86 cycle (Branfireun et al., 2020). For example, changes in organic matter cycling between the
87 catchment and the lake (Ravichandran, 2004), algal scavenging (Outridge et al., 2019), and early
88 diagenesis (Frieling et al., 2023). A decline in the total water volume of a basin may also elicit a
89 reduction in stratification (Woolway et al., 2020), during which increased mixing would ventilate
90 bottom waters and reduce organic-matter burial (Gulati et al., 2017). Conversely, a simultaneous
91 increase in total water volume and nutrient influx may increase stratification and bottom-water anoxia
92 to such an extent, that the system experiences a distinct increase in organic matter burial (Pilla et al.,
93 2020). Studies have also found catchment and basin structure to be important when considering the
94 extent to which sedimentary Hg signals reflect hydroclimate-driven variability, as both influence the
95 ease with which water is able to transport Hg to, from, and between discrete terrestrial sinks (Paine et
96 al., 2024).

97 ~~Earth's hydroclimate is highly variable in space and time (Bradley and Diaz, 2021).~~ In the short-term,
98 these interactions may manifest as annual changes in rainfall intensity and seasonality, or by sub-
99 decadal fluctuations in regional-scale climate modes (e.g., El-Nino Southern Oscillation, North Atlantic
100 Oscillation; Hernández et al., 2020). In the long-term, variability in the form of prolonged droughts
101 and/or pluvials may occur in response to global-scale atmospheric reorganization lasting centuries,
102 and changes in the planet's orbital configuration on timescales of many millennia (Bradley and Diaz,
103 2021). These wet-dry oscillations are important on a continental-scale. For example, periods of
104 extreme hydroclimate variability are known to have caused major changes in environmental
105 conditions across sub-Saharan Africa during the late Pleistocene, lasting for multiple millennia (e.g.,
106 Scholz et al., 2007).

107 Millennial-scale changes in hydroclimate may also affect the Hg cycle. Sediment cores extracted from
108 the Pacific and Atlantic oceans show low-amplitude Hg signals corresponding to orbital-scale ($>10^4$ -
109 year) changes in precipitation and rates of sediment delivery to the ocean (e.g., Chede et al., 2022;
110 Fadina et al., 2019; Figueiredo et al., 2022; Zou et al., 2021), and a growing number of terrestrial
111 successions also show Hg fluctuations coeval with climate-driven changes in local precipitation, cloud
112 formation, and ice/permafrost extent (e.g., Guédron et al., 2018; Nalbant et al., 2023; Paine et al.,
113 2024; Pan et al., 2020; Pérez-Rodríguez et al., 2018). However, few terrestrial Hg records extend
114 beyond the present interglacial (>12 ka), and even fewer come from the low-latitudes where tropical

Field Code Changed

rainforest, grassland and desert biomes are highly sensitive to millennial-scale hydroclimate variability (Bradley and Diaz, 2021; Schneider et al., 2023). Thus, our current understanding of Hg behaviour may not fully account for the impact of major, long-term hydroclimate changes on Hg transformation and transport through tropical environments (Obriest et al., 2018; Schneider et al., 2023), highlighting the need for new Hg records spanning long ($>10^3$ -year) timescales.

120

1.2.3 ~~West African Monsoon~~ Research objectives

Sedimentary records offer an opportunity to assess the impact of millennial-scale hydroclimate variability, and related effects, on the terrestrial Hg cycle. In ~~its domain, sub-Saharan Africa~~, the West African Monsoon (WAM) regulates precipitation amount and distribution, and drives long-term evolution of environmental characteristics and mineral-dust emissions (O'Mara et al., 2022; Kaboth-Bahr et al., 2021; Kuechler et al., 2013; Weldeab et al., 2007). Proxy records from ~~sub-Saharan Africa~~ this domain show that orbitally-driven variations in the strength of the WAM have frequently driven ~~severe drought events~~ distinct arid (Cohen et al., 2007; Scholz et al., 2007) and humid periods (Armstrong et al., 2023; Menviel et al., 2021) throughout the Pleistocene. These humid and arid periods have been linked to distinct changes in vegetation structure, ecosystem dynamics, and human evolution across the continent (e.g., Cohen et al., 2022; Foerster et al., 2022; Gosling et al., 2022b). In light of growing evidence for a hydroclimatic influence on the terrestrial Hg cycle (e.g., Guédron et al., 2018; Nalbant et al., 2023; Paine et al., 2024), we hypothesized that humid and/or arid periods in sub-Saharan Africa would have elicited measurable changes in the Hg cycle, producing measurable signals in regional sedimentary records. ~~This study focusses~~ Here our focus is on sediment core BOS04-5B extracted from Lake Bosumtwi, Ghana (West Africa): ~~a core that, which~~ provides a clear and continuous record of this hydroclimate variability covering the late Pleistocene (Koeberl et al., 2007).

Lake Bosumtwi is a closed system isolated from the regional groundwater network, rendering it sensitive to both short and long-term variability in rainfall, humidity, and dynamic surface processes (Shanahan et al., 2008b; Turner et al., 1996). Integrated proxy data shows that Lake Bosumtwi experienced dramatic changes in water balance, aeolian dust inputs, and biological productivity throughout its history. These changes all correspond to moisture-driven oscillations between a forest and grass-dominated catchment in response to insolation-driven variability in WAM strength, and migration of the Intertropical Convergence Zone (ITCZ) (Vinnepand et al., 2024; Gosling et al., 2022a; Miller et al., 2016; Peck et al., 2004). Focussing on the uppermost ~47 m of the Lake Bosumtwi sediment record, this study ~~aims to assess~~ es whether major shifts in local hydroclimate produced measurable changes in how Hg has been transported to, and buried within, this system since ~96 ka. By comparing our sedimentary Hg record with proxy data from archives across the African continent (e.g., Foerster et al., 2022; Scholz et al., 2007), we explored d whether hydroclimate has exerted a measurable effect on terrestrial Hg cycling in the WAM domain in over the past ~100-kyr.

152

Field Code Changed

Field Code Changed

Field Code Changed

2. Site Description

2.1. Lake Bosumtwi

Lake Bosumtwi is the only natural lake in Ghana, West Africa (6°30' N, 1°25' W) (**Fig. 1**). It occupies a 1.08 ± 0.04 Ma meteorite impact crater dated to 1.08 ± 0.04 Ma, which is one of the youngest and best preserved impact craters on Earth (Jourdan et al., 2009). The surrounding bedrock and meteorite impact target rocks are Proterozoic metagraywackes, phyllites and metavolcanic rocks of the Birimian Supergroup (~2 Ga) (Jones et al., 1981). Lake beds, soils, and breccias constitute the most recent rock formations at the site, and are associated with evolution of the crater through time (Koerberl et al. 2007). excavated in metamorphosed and crystalline rocks of the Birimian Supergroup (~2 Ga). The present-day lake is ~8.5 km in diameter, with a water depth of up to 80 m at the lake centre, and the lake water level is currently at least 120 m below the crater rim (Shanahan et al., 2007). The crater itself is ~10.5 km in diameter at the rim with steep slopes, and a well-defined spillway (~120 m above the present lake surface) marks evidence of lake overflow likely during the most recent humid period (**Fig. 1**) (Shanahan et al., 2015). The lake is meromictic, with a shallow oxycline located ~10–15 m below the water's surface (Turner et al., 1996).

The Bosumtwi basin is hydrologically closed with no external drainages, connection to the regional groundwater aquifer, river or stream inflow originating outside of the crater (**Fig. 1**) (Turner et al., 1996). Only during exceptionally high lake levels does water leave the lake, through the spillway (Shanahan et al., 2007). Approximately 300 m of sediment has accumulated in the centre of the basin originating from biological processes within the lake, progressive erosion of the crater wall, aeolian transport, and vegetation within the crater (Koeberl et al., 2005). These properties render the lake highly sensitive to changes in atmospheric processes, but also imply that Hg inputs may originate exclusively from the atmosphere (e.g., by wet deposition). Therefore, this system is ideally suited for exploring whether specific basin characteristics (e.g., depth, nutrient status, bathymetry) could also measurably affect how Hg signals are encoded in the sedimentary record.

2.1.1. West African Climate

Seasonal variability in the tropical rain belt position drives short-term (<10-year) hydroclimate change in West Africa. During boreal summer, an increase in northern hemisphere summer (June to August) insolation triggers a northward ITCZ shift, creating a pressure gradient that brings moisture eastwards from the Atlantic Ocean to western Africa. The opposite occurs in boreal winter (December to February), where the ITCZ is displaced southwards, bringing dry, aerosol-rich, continental trade winds to West Africa. Together, these seasonal shifts produce distinct annual wet (May to October) and dry seasons.

On longer (>10⁴-year) timescales, hydroclimate variability in West Africa has been linked to cyclic changes in Earth's orbital configuration. Changes in axial precession produce fluctuations in seasonal insolation above the African continent, influencing the strength of the WAM, the Walker Circulation,

the position and dimensions of the ITCZ, and the availability of continental moisture (Gosling et al., 2022b; Kaboth-Bahr et al., 2021; Trauth et al., 2021). Several studies have shown weakening of the WAM and southward migration of the ITCZ in response to high precession and/or changes in insolation gradient, producing drier conditions in West Africa and subsequent reductions in terrestrial precipitation, ecosystem productivity, and recession of terrestrial forests. High precession causes weakening of the WAM and southward migration of the ITCZ, producing drier conditions in West Africa and subsequent reductions in terrestrial precipitation, ecosystem productivity, and recession of terrestrial forests (Menviel et al., 2024). Conversely, strengthening of the WAM and a more northerly ITCZ position is documented when precession is low, bringing wetter and warmer conditions to West Africa and causing expansion of dense forests, voluminous lakes, and diverse ecosystems (Larrasoana et al., 2013; Pausata et al., 2020). During the last glacial cycle, moisture availability in West Africa also fluctuated in conjunction with the waxing and waning of high-latitude ice sheets, and their effects on sea-surface temperatures (SSTs) in the North Atlantic (deMenocal, 1995; Weldeab et al., 2007). This teleconnection exists as a function of atmospheric moisture transport and convection processes occurring in the polar and tropical regions. Low global ice volumes typically correspond to warmer North Atlantic SSTs, driving increased atmospheric moisture transport and hence more moist conditions in West Africa. Conversely, high global ice volumes generally correspond to cooler SSTs in the North Atlantic, and subsequently drier conditions in West Africa (e.g., Crocker et al., 2022; Lupien et al., 2023; Stager et al., 2011; Tjallingii et al., 2008).

2.1.2. Local hydrology and vegetation

Approximately 49% of the Bosumtwi drainage basin (area: 106 km²) is currently occupied by the lake. Situated in close proximity to the (current) ecological transition-zone between savannah in the north and moist forest in the south, Lake Bosumtwi lies directly in the seasonal migration path of the ITCZ (Nicholson, 2013). It experiences a current mean annual temperature of ~26°C, ranging between ~23°C in August to ~27°C in February, with cooler summer temperatures attributed to increased cloudiness and related reduction in incoming solar radiation (Shanahan et al., 2007). Present-day humidity ranges from ~85% in August to ~75% in January, and average annual precipitation is ~1450 mm (Turner et al., 1996). At present, the surrounding catchment is classified as a '*Tropical and Subtropical Moist Broadleaf Forest*' biome (White, 1983), meaning it is heavily forested with well-developed tropical soils, although many flat-lying areas have been converted to agriculture (e.g., maize, plantain, cocoa, and oil palm) in recent decades (Boamah and Koeberl, 2007). Before human occupation of the site, the lake was surrounded by a moist semideciduous forest, with a canopy including abundant trees from the Ulmaceae and Sterculiaceae (flowering plant) families (Miller and Gosling, 2014).

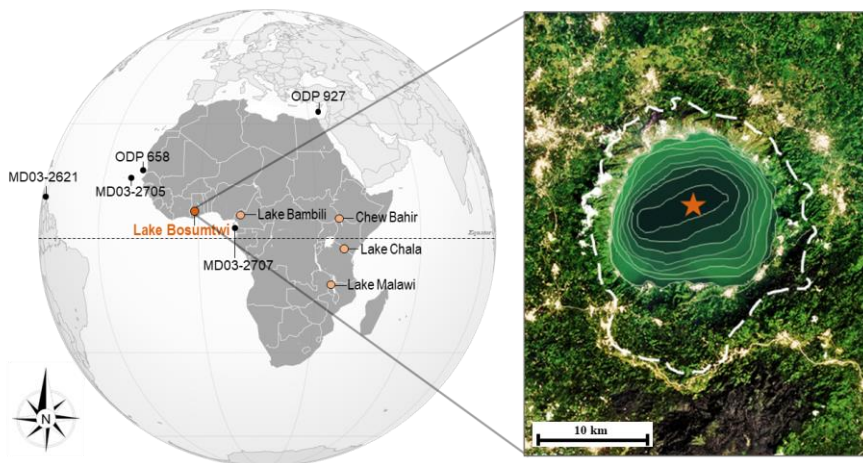


Figure 1: (Left) Location of key lake and marine sediment archives in and around Sub-Saharan Africa (SSA). (Right) An aerial photograph of Lake Bosumtwi (*copyright: NASA, 2018*), on which the location of the BOS04-5B drill site is marked as an orange star. Contours show lake bathymetry, with each step representing a 10 m depth change and culminating in a maximum depth of 75 m (Shanahan et al., 2012). The spillway notch is in the eastern rim of the crater, and the dashed white line marks the extent of the drainage divide (Brooks et al., 2005; Shanahan et al., 2006).

2.1.3. Paleoclimatic significance

Lake Bosumtwi provides an excellent record of millennial-scale hydroclimate change in West Africa. The upper ~47 m of sediment corresponds to the interval ~96 ka to present, and contains a series of distinct lithological features suggesting pronounced, climate-driven changes in lake level, catchment structure, and sediment transport processes (Vinnepand et al., 2024; Gosling et al., 2022a; McKay, 2012; Miller et al., 2016). For example, a massive, clastic-rich blue-grey clay unit is present between ~34 and 32 m depth, where TOC values drop to <1% and bulk density values increase by >60% (Scholz et al., 2007). Interpreted and referred to as Arid Interval(AI)-1 (McKay, 2012), this unit formed during extremely dry climatic conditions leading to near-total desiccation of the lake, and this interpretation is further supported by identification of a clear erosional unconformity corresponding to the age of the AI-1 unit in seismic reflection profiles (Brooks et al., 2005; Scholz et al., 2007).

Changing physical properties and geochemistry of sediments deposited prior to and following Unit AI-1 appear to reflect regional hydroclimate shifts (Scholz et al., 2007). Prior to AI-1, the presence of clastic-rich, organic-depleted sediments suggest a progressive reduction in water depth, likely in response to a (long-term) negative water balance (McKay, 2012; Shanahan et al., 2008b). Following AI-1, an abrupt reduction in clastic material concentrations, increased TOC, diagenetic carbonate, and lamination frequency all imply oxygen depletion at the sediment-water interface – evidence for a shift

Field Code Changed
Formatted: French (Switzerland)
Formatted: French (Switzerland)
Formatted: French (Switzerland)

to a positive water balance (McKay, 2012; Scholz et al., 2007; Shanahan et al., 2008a). The core also shows distinct co-enrichment in manganese (Mn) and iron (Fe) in certain intervals following AI-1, which ~~that~~ are associated with manganosiderite (Mn-rich FeCO₃) precipitation in the lake sediments. Manganosiderite requires anoxic non-sulphidic (ferruginous) pore-water conditions and high dissolved inorganic carbon concentrations to precipitate (Brumsack, 2006; Tribouillard et al., 2006), and appears as a consequence of the redox tower migrating into the water column: a response to increasing water column stratification, and overall lake level (Shanahan et al., 2006). The closed hydrology of Lake Bosumtwi means that changing water levels are likely to reflect the magnitude of precipitation variability in the region, with higher lake levels typically occurring during wetter climate intervals (Russell et al., 2003; Shanahan et al., 2008b). However, lake level may have also been influenced by secondary processes such as evaporation, and, over long time-scales, sediment infill (McKay, 2012).

3. Material and methods

3.1. BOS04-5B

Core BOS04-5B was recovered in 2004 as part of the International Continental Drilling Program (Koeberl et al., 2005) (full details in **SI1**). Our study focuses on the upper ~47 m section of a 296-m-long core extracted from deep-water (76 m) site 5 (core BOS04-5B; **Fig. 1**), which ~~that~~ extends from the present-day lake floor to the brecciated bedrock dated by ⁴⁰Ar/³⁹Ar to 1.08±0.04 Ma (Jourdan et al., 2009). Over ~67% of the full 294 m-long (~1-Myr) sediment succession is laminated (Koeberl et al., 2007), with distinctive alternating clastic, organic and carbonate laminae (Shanahan et al., 2012, 2009, 2008a). Thicker laminations are visible either as packets of light grey microturbidites, or distinct yellow and orange carbonates produced by enhanced redox-related precipitation of Fe and Mn bearing minerals (Shanahan et al., 2008a).

After drilling in 2004, core BOS04-5B was shipped to the University of Rhode Island and split. The physical properties of the full ~296 m core were measured at 2-cm intervals using a Geotek® multi-sensor core logger (Koeberl et al., 2007). After logging and imaging and at 4-cm resolution, 2 cm thick slices were removed from the core half and separated into sub-samples for multi-proxy analyses, including sediment magnetic hysteresis, x-ray diffraction mineralogy, total organic and inorganic carbon content, bulk organic carbon and nitrogen isotopes, grain size, pollen, and charcoal (e.g., Gosling et al., 2022; McKay, 2012; Miller et al., 2016). Following bulk sediment analyses, the BOS04-5B core material was transferred to the Continental Scientific Drilling (CSD) Repository in Minneapolis.

3.2. Chronology

Formatted: Font: Bold

278 Age control for the ~47 m of sediment analysed in this study is provided by the BOSMORE7 model,
279 ~~generated-presented~~ by Gosling et al. (2022). Using a combination of radiocarbon (calibrated ^{14}C ; n=
280 109), optically stimulated luminescence (OSL; n=22) and uranium-thorium (U/Th; n=5) dates as
281 independent tie-points, Bayesian modelling suggests that the upper ~47 m of sedimentation at Lake
282 Bosumtwi corresponds to the interval ~96–0 ka (full details in **ST3**) (Gosling et al., 2022a; Shanahan
283 et al., 2013). Age estimates for the AI-1 sedimentary unit are constrained by ^{14}C , OSL and U-Th
284 dating of the surrounding sediments, and suggest this unit formed between 77 and 71 (± 5) ka (Scholz
285 et al., 2007; Shanahan et al., 2008b). The duration of the event is less clear due to the excessive
286 erosion of the newly exposed crater walls and reduction in distance between the shore and 5B core
287 site (McKay, 2012) which may have led to unusually high sedimentation rates during this interval.
288 Thus, slight underestimation of sediment ages immediately following unit AI-1 may be expected.

289

290 **3.3. Sediment geochemistry**

291 **3.3.1. Mercury**

292 Total Hg (Hg_T) in the bulk sediments of core BOS04-5B was measured using the RA-915 Portable
293 Mercury Analyzer with PYRO-915+ Pyrolyzer, Lumex (Bin et al., 2001) at the University of Oxford. For
294 this study, we analysed 165 samples spanning the composite depth interval 47.7 to 0 m, with an
295 average temporal resolution of ~0.6 ka between each sample (~~range: 0.01 to 5.85 kyr~~). Dry powdered
296 sample material (45–100 mg) was heated to ~700°C, volatilizing Hg in the sample. Atomic absorption
297 spectrometry of the gases produced during pyrolysis quantifies the total Hg content of the sample. Six
298 different quantities of standard material (paint-contaminated soil – NIST Standard Reference Material
299 ® 2587) with a known Hg value of $290 \pm 9 \text{ ng g}^{-1}$ were ~~run-analysed~~ to calibrate the instrument before
300 sample analysis, and then one standard for every 10 lacustrine samples (~~supplementary data~~).
301 Calibration results accompany this article in a supplementary dataset. Long-term observations of
302 standard measurements ($n = 390$) for this instrument show average reproducibility (1 sigma) of 6% for
303 samples with $\geq 10 \text{ ng g}^{-1}$ Hg (Frieling et al. 2023). Four (2%) of the analysed samples contained very
304 low Hg contents ($< 10 \text{ ng g}^{-1}$), and likely have uncertainties $\geq 10\%$. Details of standard runs are
305 included ~~as a supplementary file in an accompanying dataset~~.

306

307 **3.3.2. Organic and inorganic carbon**

308 Quantitative values for total organic carbon (TOC) and total inorganic carbon (TIC) content were
309 measured on the same powdered sample material also analysed for Hg, using a Strohlein Coulomat
310 702 (Jenkyns and Weedon, 2013) at the University of Oxford. Analytical reproducibility for this
311 instrument was $\leq 0.2\%$ based on repeat measurements, with a detection limit of ca. 0.1–0.2 %.

312 Powdered BOS04-5B sediment samples were split into two aliquots. Weights for aliquot 1 were
313 between 50–70 mg, and aliquot 2 between 90–120 mg. Prior to coulometric analysis, aliquot 2
314 samples were furnace for 24 hours at 420°C in order to remove organic carbon fractions. Both

Formatted: Font: Bold

315 aliquots were then combusted in oxygen at 1220°C to break down the calcium carbonate and produce
316 carbon dioxide (CO₂), ~~which that~~ was fed into a solution of barium perchlorate. By producing a change
317 in solution pH from an initial value of 10.0, back titration to the original pH using electrolysis provided
318 a measure of the amount of carbon originally present – quantified by the amount of electricity required
319 to restore a pH of 10.0 and recorded in counts (Jenkyns, 1988; Jenkyns and Weedon, 2013). Counts
320 obtained for aliquots 1 and 2 were used to calculate the total carbon (TC) content of each aliquot in
321 wt.%, using the formula:

$$322 \quad TC = \frac{\text{total counts} \times 0.2}{M} \quad (\text{eqn. 1})$$

323 where M is the sample mass in mg.

324 TOC was calculated as follows:

$$325 \quad TOC = TC_1 - TC_2 \quad (\text{eqn. 2})$$

326 where TC₁ and TC₂ represent the TC values obtained for aliquots (1) and (2), respectively. TC₂
327 represents the TIC value for the sample. Our TOC curve was then compared with measurements
328 previously obtained for BOS04-5B (on discrete samples): to assess the broader reproducibility of our
329 results (Fig. SF1).

330

331 3.3.3. Authigenic carbonates

332 The BOS04-5B succession contains variable amounts of diagenetic carbonates, predominantly
333 (mangano-)siderite (**Fig. SF2**) (McKay, 2012). Siderites commonly form in freshwater settings at
334 shallow sediment depths under anaerobic (anoxic) conditions accompanied by organic-rich sediments
335 (Armenteros, 2010; Seabag et al., 2018). However, they can also preclude accurate measurement of
336 organic carbon content in lacustrine sediment via pyrolysis- or furnace-based methods, causing
337 systematic overestimation of total organic carbon (TOC) due to the fact that thermal decomposition of
338 siderite typically starts at temperatures <420°C (Seabag et al., 2018), which is lower than that which is
339 used to remove the organic fraction on the Coulomat (Jenkyns, 1988). To assess whether siderite-
340 associated carbon had an appreciable impact on the TOC measurements, we also analysed the
341 carbon release from sixteen BOS04-5B samples spanning a range of low to high XRF-derived Mn
342 counts (i.e., covering the possible range of (mangano-)siderite contents) using a weak acid (warm 5%
343 HCl) treatment, following established methodologies (**ST5**: Brodie et al., 2011; Vinduřková et al.,
344 2019). ~~Full details are provided in S6.~~ Comparison of acid-treated and furnace samples showed no
345 systematic offset nor a clear correlation with the Mn counts from XRF data (**Fig. SF2c**), suggesting
346 that the carbon release from siderite did not appreciably bias TOC measurements.

347

348 3.3.4. Scanning X-Ray fluorescence

Formatted: Font: Bold

The Hg data for core BOS04-5B generated in this study are paired with unpublished x-ray fluorescence (XRF) data (McKay, 2012). The bulk elemental composition of the core was quantified using the Itrax® scanning XRF analyser at the Large Lake Observatory at the University of Minnesota. Core material was analysed at 1-cm-resolution with 60 sec count times, and a Mo X-ray source run at 30 kV and 20 mA. Analytical and correctional procedures for element abundance measurements covering the upper ~159 m (~500-kyr) of BOS04-5B are fully described in S7. To mitigate any effects arising from changes in the physical properties of the BOS04-5B sediments (e.g. compaction) and/or the measurement times, we applied a centred-log ratio (clr) transformation to the measured XRF values. The centred log-ratio (clr) values are calculated by dividing the intensities of an element by the average of the intensities obtained on all selected elements, and are dimensionless such that positive values are generated for elements with high intensities, and vice versa (Bertrand et al., 2024). Therefore, elements (X) subject to this transformation are presented as their centred-log ratio value (X_{clr}).

3.4. Mercury normalization

It is common practice to assess both total Hg concentration (Hg_T) and normalised Hg (Hg/X) with the aim to reduce, at least partially, the potential impact of variability in a dominant carrier/host phase (X) on Hg_T (Sanei et al., 2012; Shen et al., 2020). Organic matter (here expressed as TOC) is commonly considered the primary host phase of sedimentary Hg (Ravichandran, 2004). However, variability in Hg_T may also be associated with variability in the abundance of detrital minerals, usually detected by a correlation between Hg and detrital elements such as Al or K (Paine et al., 2024; Them et al., 2019), and very rarely in sulphate-limited (lacustrine) sediments, sulphides (Benoit et al., 1999; Han et al., 2008). Exploration of Hg signal variability relative to distinct shifts in the abundance, contribution and/or sources of host phases can therefore elucidate the timing and magnitude of shifts in lake hydrology, sedimentation regime, and geochemistry, and whether these are connected to changes in the Hg cycle or sediment composition changes (Paine et al., 2024).

To isolate the effects of local depositional and/or transport processes on Hg signals recorded in the sediments of Lake Bosumtwi, we normalised Hg_T values to organic matter (TOC) and detrital mineral abundance estimated from potassium (K) intensities; with the assumption that the strongest positive-sloped linear correlation with Hg_T among these elements signals the most likely dominant impact of host phase variability in that section of the core. To account for differences in resolution between Hg and XRF data, K measurements were averaged to obtain a K value corresponding to the interval covered by each discrete Hg sample (~0.5 cm thickness).

3.5. Mercury accumulation

The total Hg mass accumulation rate (Hg_{AR}) in core BOS04-5B was calculated from:

$$Hg_{AR} = Hg_T (DBD \times SR) \quad (eqn. 3)$$

where Hg_{AR} is in $mg\ m^{-2}\ kyr^{-1}$, Hg_T is the total mercury concentration ($mg\ g^{-1}$), DBD is the dry bulk density ($g\ m^{-3}$), and SR is the sediment accumulation rate ($m\ kyr^{-1}$). Values for Hg_{AR} are also calculated with respect to the median age estimate for each sample. We do not present maximum and minimum Hg_{AR} values here, but note that uncertainties increase with depth due to increasing uncertainties in sedimentation rates, which are calculated based on the BOSMORE7 age model and average $\sim 0.08\ cm\ yr^{-1}$ ($0.02\text{--}0.3\ cm\ yr^{-1}$).

DBD values were calculated using measurements obtained by loss-on-ignition (McKay, 2012; Shanahan et al., 2013), using the formula:

$$DBD = M_{solid}/V_{total} \quad (eqn. 4)$$

where M_{solid} is the mass of dry solid material (g) in each sample, and V_{total} is the volume of each respective sample ($0.5\ cm^3$). To calculate M_{solid} , the proportion of clastic material was multiplied by an assumed grain density value ($2.6\ g\ cm^{-3}$) representative of a mixture of common sedimentary minerals (e.g. quartz, clay minerals, clastic; typically range of 2.6 to $3\ g\ cm^{-3}$) and the total volume. The proportion of clastic material was calculated by first accounting for the proportion of water and organic matter (measured by McKay (2012) and Shanahan et al. (2013) in each sample and assuming the residual was all clastic material. DBD values generally increase with core depth, which reflects the impact of increasing sediment compaction and dewatering with age (Shanahan et al., 2013). Calculated values of DBD average $1.15\ g\ cm^{-3}$, which is broadly consistent with measurements taken from other African lake sediment successions of similar age ($<100\ ka$), composition (silty clays between $0.6\text{--}1.1\ g\ cm^{-3}$), and structure (high porosity) (e.g., Cohen et al., 2016; Scholz et al., 2007).

3.6. Statistical analyses

Two statistical analyses were used in order to more quantitatively explore the timing, and expression of signals recorded in the BOS04-5B Hg_T dataset. First was a simple linear Pearson's correlation analysis (ST6), from which correlation coefficients (r) were calculated to indicate the direction and strength of the association between Hg ($n = 157$), and a suite of geochemical proxies also measured in the core. Second was a change point analysis (ST7), to determine whether distinct changes in mean values of Hg_T occur within the record using PAST v.4.16 software (Hammer et al. 2001). This software employs a Bayesian Markov chain Monte Carlo (MCMC) approach, which was run on default settings with a total of 1 million MCMC simulations were run for each test and a maximum of ≤ 10 changepoints. The extent to which similar processes influenced the concentration of Hg_T, TOC, K, and detrital matter were also explored, and correlations were subdivided based on visual examination of the Hg_T records (and supported by changepoint analyses). The significance of all correlations was assessed using a Student's t-test, which showed that $\sim 50\%$ of the assessed geochemical combinations were significant at $p < 0.01$.

Formatted: Font: (Default) Arial, 12 pt, Not Italic

Formatted: List Paragraph, Outline numbered + Level: 2 + Numbering Style: 1, 2, 3, ... + Start at: 1 + Alignment: Left + Aligned at: 0 cm + Indent at: 1.27 cm

Formatted: Font: (Default) Arial, 12 pt, Bold, Font color: Custom Color(RGB(0,101,153))

Formatted: Font: (Default) Arial, 10 pt, Not Italic

Formatted: Font: (Default) Arial, 10 pt, Not Italic, Subscript

Formatted: Font: (Default) Arial, 10 pt, Not Italic

Formatted: Font: Bold

Formatted: Font: (Default) Arial, 10 pt, Not Italic

Formatted: Font: (Default) Arial, 10 pt, Not Italic

Formatted: Font: (Default) Arial, 10 pt, Not Italic, Subscript

Formatted: Font: (Default) Arial, 10 pt, Not Italic

Formatted: Font: (Default) Arial, 10 pt, Not Italic

Formatted: Font: (Default) Arial

421 **4. Results**

422 Core BOS04-5B from Lake Bosumtwi shows distinct fluctuations in total sedimentary Hg
423 concentration (Hg_T) throughout the ~47 m succession. Values range from 10 to 370 $ng\ g^{-1}$ (median:
424 58 $ng\ g^{-1}$) (**Fig. 2**). The Hg_T curve broadly tracks that of TOC, which shows similarly pronounced
425 variability ranging between 0.1 to 23 wt. % (median: 6.5 wt. %) (**Fig. 2**), and peaking between 5.2 and
426 3 m depth. Calculated Hg accumulation rates (Hg_{AR}) do not follow the same pattern as Hg_T and TOC.
427 Ranging between 2.9 and 460 $mg\ m^{-2}\ kyr^{-1}$, calculated values instead broadly track the sedimentation
428 rate curve presented in **Figure 2**. Large peaks in Hg_{AR} are visible between 8 and 6 m depth and then
429 again between 2 and 0 m, and these Hg_{AR} peaks are both coeval with reductions in TOC below ~10
430 wt.%. The lowest Hg_{AR} values are recorded in the lower core section between ~47 and 34 m depth.

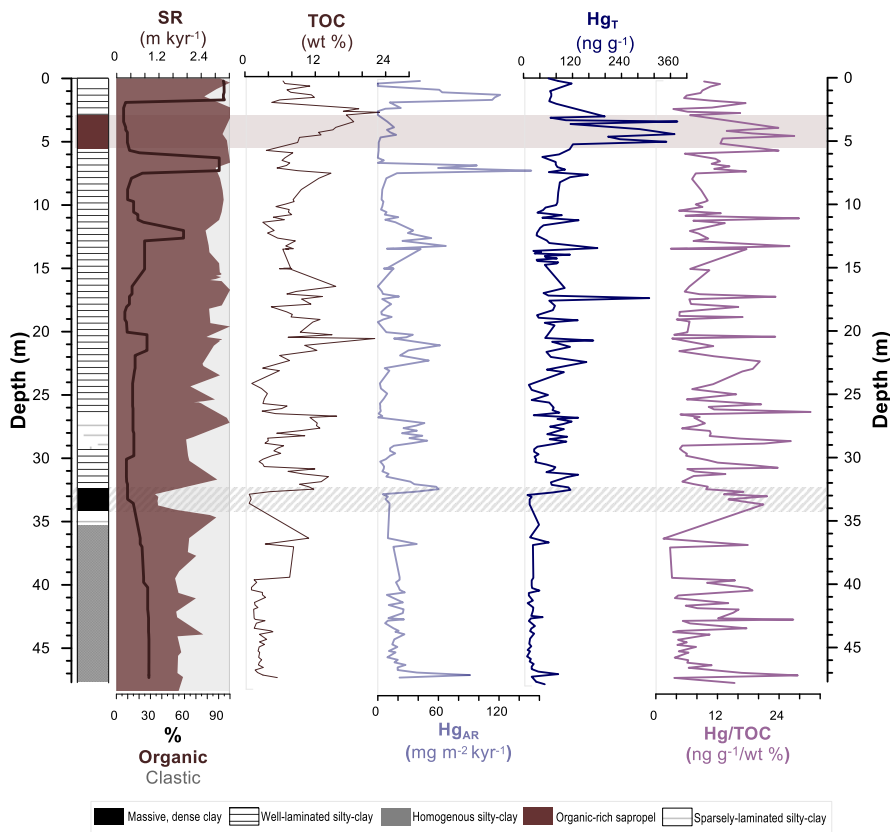


Figure 2: Depth-resolved profiles of total organic carbon (TOC), total Hg (Hg_T) and Hg accumulation rate (Hg_{AR}) profiles obtained for core BOS04-5B from Lake Bosumtwi in this study, relative to key lithofacies and sedimentological data including records of sedimentation rate (SR; *this study*), and the proportion of biogenic to terrigenous material (% organic) within the core (McKay, 2012). A distinct lake low stand referred to as Arid Interval

1 (AI-1) based on seismic profiles and sedimentological data is marked between 33.5 and 32.8 m depth (grey dashed shading; McKay, 2012; Scholz et al., 2007). Limited samples were available between ~39 and 34 m depth (Fig. SF1). Sapropel layer Unit S1 is marked between 3–5.5 m depth (brown shading; Russell et al., 2003; Shanahan et al., 2008a; Talbot and Johannessen, 1992). We also present ratios of Hg_T to TOC, following evidence for a positive correlation between the two compounds ($r = 0.64$; $r^2 = 0.42$) (see section 4.1).

Changing Hg signals in Lake Bosumtwi correspond to measurable changes in lake sedimentation. From ~47 to 32 m depth, low amplitude, muted variability in both Hg_T and Hg_{AR} corresponds to a homogeneous sequence of silty-clay sized material generally depleted in TOC, S, and high in detrital materials. No clear changes in Hg_T nor Hg_{AR} are visible during AI-1 (34 – 32 m core depth), however, variability in Hg concentration increases immediately following this interval. From ~32 m to the core top, sediments show a progressive increase in Hg_T punctuated by several clear peaks, and more pronounced fluctuations in Hg_{AR} (Fig. 2). This shift in Hg behaviour tracks a broad increase in the organic content of the core compared to clastic, reflected by increasing TOC and decreasing K profiles (Fig. 2). The clearest expression of this correspondence is seen between 5.2 and 3 m, whereby the highest Hg_T values correspond to the organic-rich sapropel Unit S1.

Studying time-resolved changes in lake sediment Hg concentration provides a valuable opportunity to study changes in the pre-industrial Hg cycle, how these changes translate to measurable sedimentary signals, and their links to local and regional-scale environmental variability (Cooke et al., 2020). Two mechanisms emerge as plausible drivers of Hg variability in Lake Bosumtwi (Fig. 2). First is external changes in net Hg input to the system, and second is organic matter (host) availability.

Discussion

Studying time-resolved changes in lake sediment Hg concentration provides a valuable opportunity to study changes in the pre-industrial Hg cycle, how these changes translate to measurable sedimentary signals, and their links to local and regional-scale environmental variability (Cooke et al., 2020). From the data presented in Figure 2, two mechanisms emerge as plausible drivers of Hg variability in Lake Bosumtwi. First is external changes in net Hg input to the system, and second is organic matter (host) availability. Both are explored in the discussion below.

4.1. Lacustrine host phases of mercury

An overall positive association between Hg_T and TOC ($r = 0.64$; $r^2 = 0.42$) suggests that Hg variability may be associated with organic carbon variability in Lake Bosumtwi. However, it is noteworthy that detrital materials (e.g., K_{cl}) show negative correlations with both TOC ($r = -0.59$; $r^2 = 0.34$) and Hg ($r = -0.57$; $r^2 = 0.32$) so that the Hg-TOC correlation may reflect, in part, a correlation imposed by variable clay-dilution of both Hg and TOC. An overall positive association between Hg_T and TOC ($r^2 = 0.42$) suggests that Hg variability may be associated with organic carbon variability in Lake Bosumtwi. However, it is noteworthy that detrital materials (e.g., K; $r^2 = 0.34$) show negative correlations with

TOC and Hg (Fig. 3b) so that the Hg-TOC correlation may reflect, in part, a correlation imposed by variable clay dilution of both Hg and TOC. The broad statistical link between Hg and TOC is supported by evidence for large Hg_T and Hg_{AR} peaks in core sections containing high TOC concentrations, most markedly in the upper sections (Fig. 2), and the relationship between Hg_T and TOC also strengthens following deposition of Al-1 (Fig. 3a, S33b). However, the highest Hg_T values are not always recorded in the most TOC-enriched sediments, nor are TOC-depleted sediments also depleted in Hg_T (Fig. 2). Dilution of Hg by organic matter is unlikely to be the cause (Machado et al., 2016), nor can shift from an organic to detrital-dominated host-phase regime account for these signals, given that intervals characterised by an overall negative Hg and TOC correlation are coeval with similarly negative values for Hg and K_{clr} (Fig. S3, SF4). More likely is that they reflect changes in net Hg flux to the system, and hence the amount of Hg being supplied to (and sequestered in) Lake Bosumtwi.

A negative overall correlation between Hg_T and K_{clr} is apparent throughout the record ($r = -0.57$; $r^2 = 0.32$; Fig. 3b, SF4). A negative overall correlation between Hg_T and K is apparent throughout the record ($r^2 = 0.34$; Fig. 3a). Other robust proxies for the proportion of detrital and autochthonous components in biogenic-rich sediments include Fe, Ti, Rb, and Al (SF5) (Grygar et al., 2019). Strong correlations between K_{clr} , K and these detrital elements confirm this is likely also the case in Lake Bosumtwi (Fig. 3b), with enrichment of detrital materials in this core reflecting enhanced erosion and sediment transport to the BOS04-5B drill site (McKay, 2012; Shanahan et al., 2012). Moreover, the significant negative correlations between TOC, Hg_T , and all elements associated with detrital components (K_{clr} , Ti_{clr} , Rb_{clr} , and Al_{clr}) (K, Ti, Rb, and Al) (Fig. 3b) suggest that detrital matter did exert a control on Hg_T . However, instead of increasing Hg, the negative correlation with detrital material suggests that 'Hg-depleted' detrital materials diluted the concentration of both Hg and its suggested host (TOC). Variations in both the detrital and Hg flux may also explain the somewhat counterintuitive decoupling of Hg_T and Hg_{AR} in some intervals, for example, between ~10 and 6 m depth (Fig. 2). Dilution-driven alteration of the sedimentary Hg record may be a common feature for depositional systems where supply of Hg is ultimately limited by atmospheric inputs (e.g., Chede et al., 2022).

Strong correlations between Hg_T and Mn_{clr} , and Hg_T and Fe_{clr} (redox sensitive elements) are also absent in BOS04-5B (Fig. 3). The majority of the examined record is marked by the presence of laminations, suggesting anoxic conditions dominate throughout (Shanahan et al. 2008). Although this means that redox changes were likely subtle, the coeval presence of siderite has potential implications for Hg through, for example, its influence on Hg reduction (e.g., Ha et al. 2017). Fe is a major component of siderite, but it is also an important component of the detrital material that washes into Lake Bosumtwi and also potentially other redox-sensitive minerals precipitated in the lake and sediment pore waters (Shanahan 2006; Shanahan et al., 2008; 2009). In this record, we therefore test the relation between Hg_T and Mn peaks. Pronounced Mn enrichments signal periods of (mangano)siderite formation, and this constitutes the clearest indicator of (subtle) pore water redox changes (McKay, 2012; Shanahan et al., 2008). Moreover, siderite specifically may be involved in Hg cycling through its potential to reduce Hg (e.g., Ha et al. 2017). Overall, the lack of evidence for

Formatted: Subscript

substantial redox changes from ubiquitous laminations and the absence of a strong correlation between Mn and Hg_T suggests that Hg concentrations in Lake Bosumtwi were not appreciably influenced by changes in redox conditions, nor the diagenetic effects signalled by these elements. Clear correlations between Hg_T and Mn, and Hg_T and Fe (redox sensitive elements) are also absent in this record (Fig. S4), suggesting that Hg concentrations in Lake Bosumtwi was not appreciably influenced by changes in redox conditions or diagenetic effects signalled by these elements.

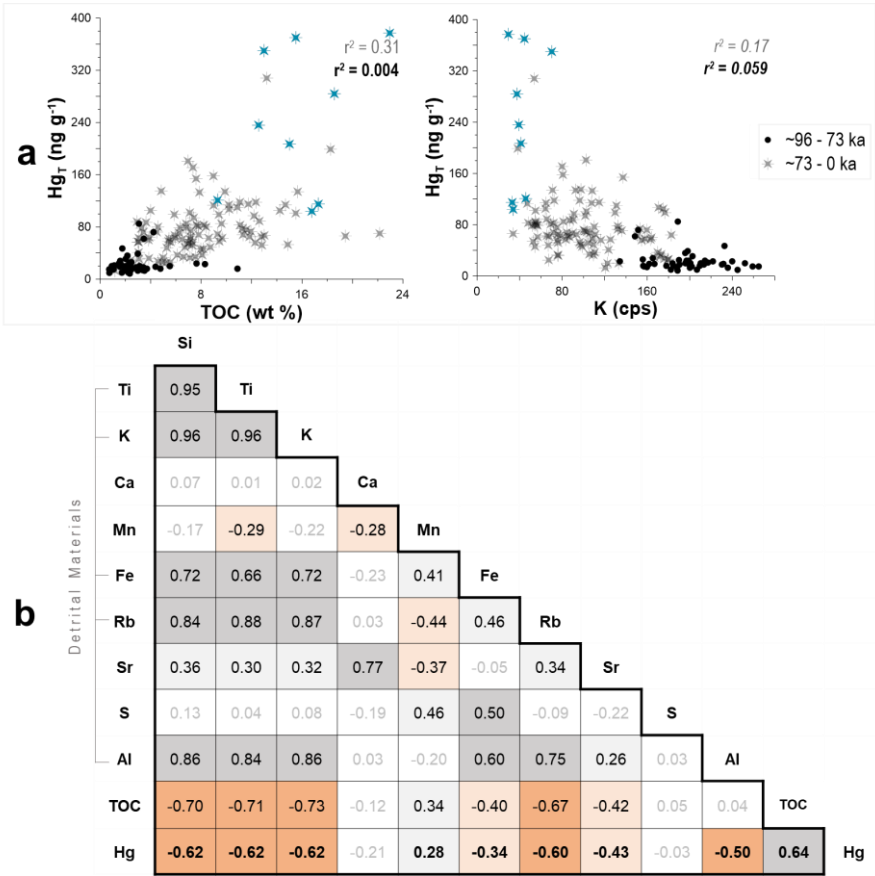


Figure 3: (a) Comparison of host-phase relationships in Lake Bosumtwi between ~96 and 73 ka (black circles), and between ~73 and 0 ka (stars). We assess the Hg_T record for this lake relative to total organic carbon (TOC) values measured in this study, and detrital minerals (estimated by potassium (K)) concentrations measured by McKay (2012). R-squared (r^2) values for each interval are also given, with italic formatting indicating a negative relationship. Stars marked in teal correspond to deposition of sapropel unit 1 (S1) in BOS04-5B. (b) Full-core correlation (Pearson's r) matrix for Hg, total organic carbon (TOC) (this study),

Formatted Table

and a suite of trace elements measured in BOS04-5B by XRF (McKay, 2012). Higher r values suggest that similar processes influence the concentration of the two elements in focus. Grey shading marks positive correlations (light: >0.25 , dark: >0.5), and orange shading marks negative correlations (light: <-0.25 , dark: <-0.5). Unshaded boxes mark weak/negligible correlations (between 0 and 0.25, and 0 and -0.25), with values greyed-out for clarity. All remaining values are presented with black text, with those in this range related to Hg in the boldest type.

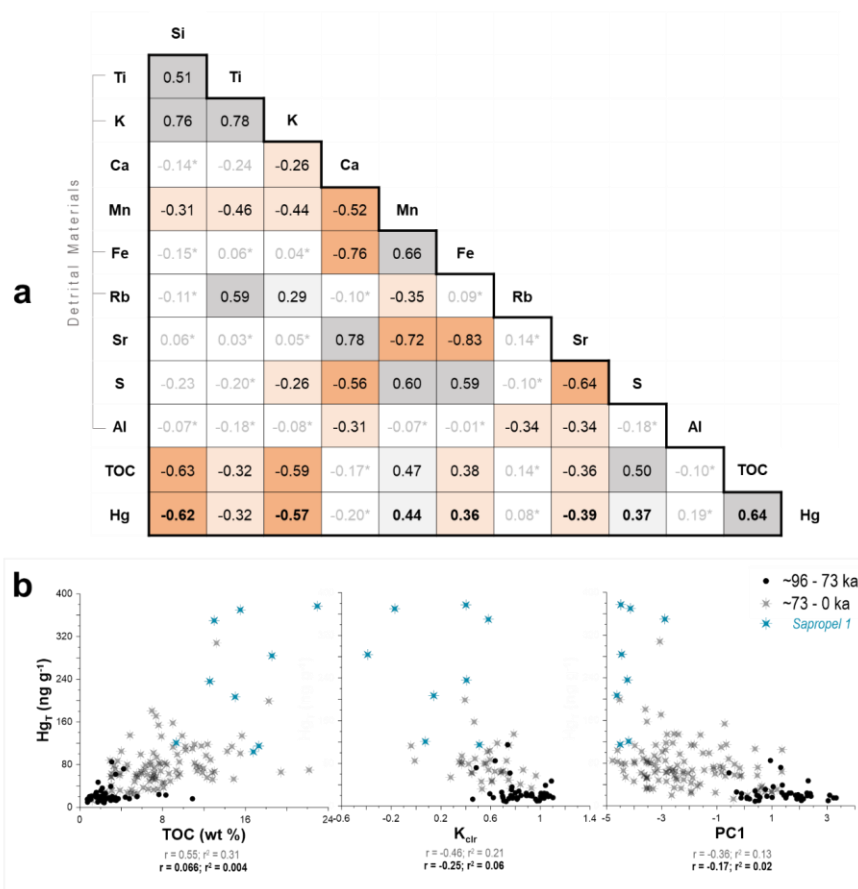


Figure 3: (a) Full-core correlation (Pearson's r) matrix for Hg, total organic carbon (TOC) (this study), and a suite of clr-transformed XRF data measured in BOS04-5B by XRF (McKay, 2012). Sample size (n) was 157 for each analysis, and $>50\%$ of the assessed trace element combinations were significant ($p < 0.01$). Those combinations that were not are marked with an asterisk (*). Grey shading marks positive correlations (light: >0.25 , dark: >0.5), and orange shading marks negative correlations (light: <-0.25 , dark: <-0.5). Unshaded boxes mark weak/negligible correlations (between 0 and 0.25, and 0 and -0.25), with values greyed-out for clarity. All remaining values are presented with black text, with those in this range related to Hg in the boldest type. **(b)** Comparison of relationships in Lake Bosumtwi between ~96 and 73 ka (black circles), and between

~73 and 0 ka (stars). Relationships presented here are between Hg_T , total organic carbon (TOC), detrital minerals (estimated by potassium (K) concentrations; McKay (2012), and principal component 1 (PC1) of the BOS04-5B XRF data, in which 39% of total variance is strongly associated with terrigenous elements (McKay, 2012). R (r) and r-squared (r^2) values for each interval are also given, and Student's t-testing showed that the significance of all correlations were significant at $p < 0.01$. Stars marked in teal correspond to deposition of sapropel unit 1 (S1) in BOS04-5B.

5. Discussion

4.2.5.1. Environmental drivers

Time resolved Hg_T and Hg_{AR} profiles generated from the sediments of Lake Bosumtwi show two broad periods of differing Hg behaviour: (1) ~96 – 73 ka (low Hg_T and Hg_{AR}) and (2) ~73 – 0 ka (moderate/high Hg_T , and large fluctuations in Hg_T and Hg_{AR}) (**Fig. 4**). Each corresponds to different lake level evolution trends with broadly decreasing lake level between ~96 and 73 ka (although with a substantial rise between 95 and 80 ka), and rising from ~73 to 0 ka (**Fig. 4**). Lake Bosumtwi's hydrology is controlled by a balance between direct precipitation and runoff with water removal limited almost entirely to evaporation; exceptions being rare transient overspilling events (Turner et al., 1996). Taking this unique hydrology into account, our discussion below explores how different environmental processes relate to changes in Hg behaviour during these two discrete intervals, and how the significance of these processes may have changed through time.

Formatted: List Paragraph, Outline numbered + Level: 1 + Numbering Style: 1, 2, 3, ... + Start at: 1 + Alignment: Left + Aligned at: 0 cm + Indent at: 0.63 cm

Formatted: Font: (Default) Arial, 14 pt, Bold

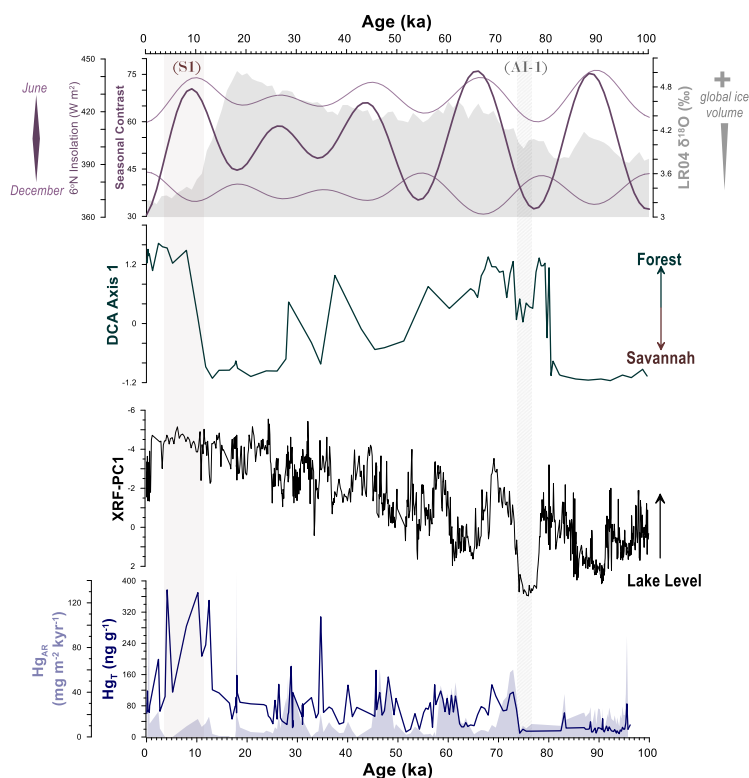


Figure 4: Comparison of key proxy datasets. Included are (from bottom to top), total mercury (Hg_T) and mercury accumulation rate (Hg_{AR}) for Lake Bosumtwi from this study (see [section 5.1](#)), the first principal component (PC1) of the BOS04-5B XRF data (39% of total variance, interpreted as an indicator of lake level changes; McKay, 2012), forest (woody) taxa abundance (presented as DCA Axis 1; Gosling et al., 2022a; Miller et al., 2016), and insolation at 6°N (location of Lake Bosumtwi) in June (summer) and December (winter) calculated following the astronomical solution presented by Laskar et al. (2004) (accessed via <https://vo.imcce.fr/insola/earth/online/earth/online/index.php>), and used to calculate seasonal insolation contrast. Also shown is a record of benthic foraminiferal calcite $\delta^{18}O$ (‰) derived from the LR04 global stack) as a proxy for ice volume, with cold glacial stages defined by high $\delta^{18}O$ ratios (Lisiecki and Raymo, 2005a). Proxy data are all presented on the BOSMORE7 chronology. Unit AI-1 is marked between 33.5 and 32.8 m depth (grey shading; Brooks et al., 2005; Scholz et al., 2007), and sapropel layer Unit S1 is marked between 3–5.5 m depth (brown shading; Shanahan et al., 2012, 2006).

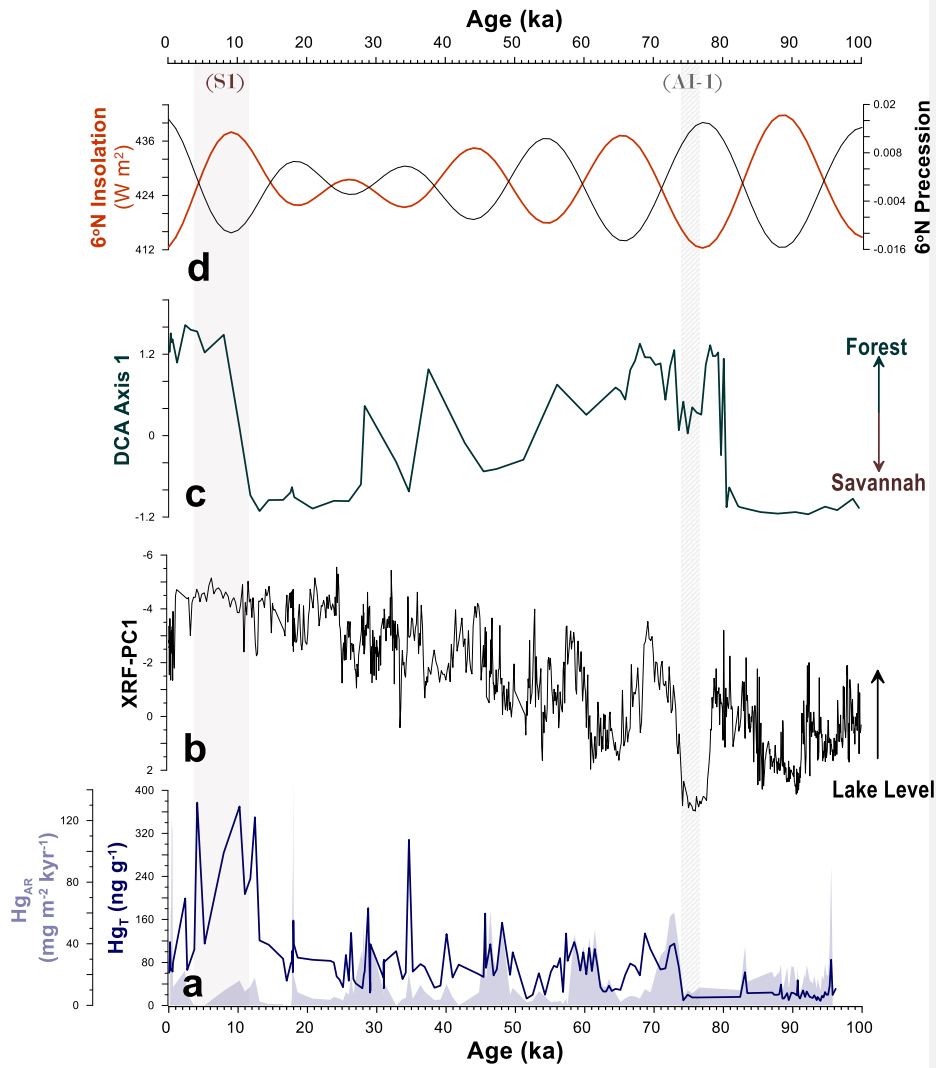


Figure 4: Comparison of key proxy datasets. **(a)** Total mercury (Hg_T) and mercury-accumulation rate (Hg_{AR}) for Lake Bosumtwi from this study, chosen as the most appropriate proxies for Hg variability in this core (see **section 5.1**). **(b)** The first principal component (PC1) of the BOS04-5B XRF data (39% of total variance) is strongly associated with terrigenous elements, and so interpreted as an indicator of lake level changes (McKay, 2012). **(c)** Forest (woody) taxa abundance (presented as DCA Axis 1; Gosling et al., 2022a; Miller et al., 2016). Lack of data for woody taxa presence is assumed to imply a savannah-dominated regional landscape. **(d)** Annual mean insolation and precessional variability at 6°N latitude, calculated following the astronomical solution presented by Laskar et al. (2004) (accessed via: <https://vo.imcce.fr/insola/earth/online/earth/online/index.php>). Orbital precession

broadly induces millennial-scale (~19 to 23 kyr) fluctuations in insolation, and enhanced precessional amplitude has been linked to more severe hydroclimatic extremes in West Africa throughout the Pleistocene (Scholz et al., 2007). Proxy data are all presented on the BOSMORE7 chronology. Unit AI-1 is marked between 33.5 and 32.8 m depth (grey shading; Brooks et al., 2005; Scholz et al., 2007), and sapropel layer Unit S1 is marked between 3–5.5 m depth (brown shading; Shanahan et al., 2012, 2006).

4.2.1.5.1.1. Arid conditions (~96 to 73 ka)

Both Hg_T and Hg_{AR} show muted variability between ~96 and 73 ka (Fig. 4a). The presence of more clastic-rich/organic-depleted sediment (Fig. 4b), and reductions in tree pollen are both typical of a savannah-dominant, more open landscape (Fig. 4c), and so suggest generally arid conditions within the lake and its catchment prior to ~73 ka. These conditions would favour pronounced reductions in lake level (McKay, 2012; Miller et al., 2016; Scholz et al., 2007), and are consistent with a 24 – 38% reduction in local rainfall as estimated by water balance modelling (Shanahan et al., 2008b). Reductions in lake level could facilitate an increase in water column vertical mixing, ventilation of bottom waters, more efficient breakdown of organic matter, and simultaneous sediment dilution by a sudden increase in eroded material fluxes (McKay, 2012; Scholz et al., 2007; Shanahan et al., 2012) – all of which could lead to a reduction in organic matter (host-phase) concentration. Indeed, several meromictic lakes have shown reduced organic matter content as a function of better ventilation and lower productivity during ‘shallow’ conditions (Katsev et al., 2010; Schultze et al., 2017), and new evidence suggests that changes in organic matter oxidation may produce comparably distinct changes in Hg sequestration (Tisserand et al., 2022).

The absence of a clear change in Hg_{AR} between ~96 and 73 ka might also reflect changes in the balances of Hg cycling in the lake. Lake Bosumtwi is a hydrologically closed system that receives >80% of its water from rainfall directly on the surface, meaning its hydrology and sedimentation regime is extremely sensitive to variability in precipitation and precipitation-evaporation balance (Shanahan et al., 2007; Turner et al., 1996). Thus, low Hg_T and Hg_{AR} values may reflect a reduction in wet deposition of atmospheric Hg at the Lake Bosumtwi site by precipitation, while Hg evasion back to the atmosphere remains high due to evaporation in the consistently warm, tropical temperatures (Schneider et al., 2023). Depletion of sedimentary Hg during drier climate intervals are documented in several other late Quaternary-age records, where they are interpreted as signs of a net reduction in Hg input relative to loss/evasion (e.g., Hermanns and Biester, 2013; Pompeani et al., 2018; Schneider et al., 2020; Schütze et al., 2021, 2018).

Desiccation of Lake Bosumtwi between ~75 and 73 ka (AI-1) corresponds to evidence for severe depletion of organic matter, and enrichment of detrital materials within the sediments (Fig. 2). Although a detailed characterization of local soil and bedrock Hg contents is currently lacking for Lake Bosumtwi, these changes in sediment composition (lower TOC, higher K) and low overall sedimentation rates are unaccompanied by coeval changes in Hg_{AR} (Fig. 2). In certain cases, one

Field Code Changed

Formatted: German (Switzerland)

Formatted: German (Switzerland)

would typically expect that the near-complete desiccation of a steep-sided lake would 'focus' trace metals (including Hg) at the central coring site, particularly during lake recessions following erosion of exposures around the crater rim (Blais and Kalff, 1995; Engstrom and Rose, 2013). However, evidence for low Hg burial both prior to and during AI-1 in Lake Bosumtwi suggests that over multiple millennia, changes in Hg supply to the BOS04-5B drill site were predominantly driven by atmospheric inputs, with minimal contribution from catchment-sourced materials.

558

559 **4.2.2.5.1.2. Humid conditions (~73 to 0 ka)**

560 The magnitude and frequency of variability in Hg_T visibly increases at ~73 (± 5) ka (Fig. 4). The
561 quantitative significance of this shift is supported by changepoint analysis of the BOS04-5B dataset,
562 which demonstrates a clear and step-wise shift in mean Hg_T values between ~75 and 73 ka (Fig.
563 SF3). It also occurs in conjunction with an increase in the lake's water level (Fig. 4b), which is
564 corroborated by a statistically significant relationship between PC1 (lake level indicator; McKay,
565 2012), and Hg_T in our record (Fig. 3b - $r = -0.36$; $r^2 = 0.13$). The magnitude and frequency of
566 variability in Hg_T and Hg_{AR} increases at ~73 (± 5) ka. This shift is coeval with an increase in the lake's
567 water level (Fig. 4b), and. Furthermore, changing sedimentary TOC, terrigenous material, and pollen
568 concentrations all corroborate a broad increase in local moisture availability, temperature, and
569 humidity following deposition of the AI-1 unit (Fig. 4): a signal that coincides with the transition into the
570 warmer Holocene interglacial, marked by reduced global ice volume and increased sea surface
571 temperatures in the North Atlantic (McKay, 2012; Scholz et al., 2007; Shanahan et al., 2008b). Our
572 data also shows a simultaneous increase in Hg_T , Hg_{AR} , and a decrease in detrital material
573 concentrations following ~73 ka (Fig. 4b, S5), suggesting that Hg supply temporarily exceeded the
574 diluting effects of clastic materials following lake level rise.

575 Lake deepening generally increases water column stratification, limiting the effects of vertical
576 transport processes such as turbulent energy generated by surface winds and currents (Gulati et al.,
577 2017). Deeper, more anoxic conditions are therefore typically associated with more effective organic
578 carbon burial (Gulati et al., 2017; Schultze et al., 2017), coupled with more distinct formation of
579 distinct laminations (Zolitschka et al., 2015) and precipitation of authigenic carbonates such as
580 siderites (Swart, 2015). Given that elevated Hg_T and Hg_{AR} correlate most closely with TOC
581 enrichment in Lake Bosumtwi following ~73 ka (Fig. 3a), this could suggest that Hg drawdown was
582 moderated by an increase in organic matter availability and preservation, as an indirect function of
583 bottom water deoxygenation. Evidence for an inverse relationship between sedimentary Hg
584 concentration and hypolimnion oxygen content has been identified in a number of meromictic lake
585 systems across the world (e.g., Schultze et al., 2017; Tisserand et al., 2022), and provides further
586 support for our interpretation.

587 Geochemical evidence suggests sedimentary oxygen depletion became progressively greater in Lake
588 Bosumtwi following ~73 ka, culminating with sapropel formation between 12.4 and 3.7 ka. This unit
589 contains clear Hg_T enrichments relative to the rest of the core (FigS. 2, 4a, SF3), is extremely rich in

Formatted: Subscript

Formatted: Font: Bold

Formatted: Subscript

Formatted: Font: Bold

Formatted: Font: Bold

590 organic matter (~15-20%), and contains a high concentration of blue-green algae *Anabaena* deposits
 591 (Russell et al., 2003). Sapropelic layers have emerged as key sites of Hg enrichment from a suite of
 592 marine and lacustrine-based studies, which suggest this may be due to changes in productivity,
 593 sediment oxygenation, and diagenetic processes (e.g., Frieling et al., 2023; Gehrke et al., 2009; Jeon
 594 et al., 2020). Scavenging of Hg from the water column by algae is also a process now recognised as
 595 an important driver of Hg export to lacustrine sediments; particularly in systems where primary
 596 productivity, organic matter production, and burial capacity is high (Outridge et al., 2007; Biester et al.,
 597 2018; Schütze et al., 2021). These conditions are met in Lake Bosumtwi following ~73 ka, meaning
 598 the observed changes in sedimentary Hg_T could be linked to elevated rates of scavenging, as a
 599 function of enhanced primary productivity.

600 In closed-basin lakes where fluxes of organic material from the catchment (e.g., soils and vegetation)
 601 are minimal, measurable changes in sedimentary Hg concentration would require a simultaneous
 602 increase in Hg fluxes to the system: to counterbalance Hg depletion by scavenging, methylation, or
 603 evasion back to the atmosphere (e.g., Bravo et al., 2017; Hermanns et al., 2013; Outridge et al.,
 604 2007; Schütze et al., 2021). For Lake Bosumtwi, these direct inputs may have come from
 605 precipitation, and/or from increased flux of charcoal into the lake following local wildfire events (Cooke
 606 et al., 2020).

607 Lake Bosumtwi records evidence for an increase in local precipitation following ~73 ka. Model and
 608 proxy-based data show that the precipitation-evaporation balance is directly coupled to lake level in
 609 this system, such that lake deepening occurs as a function of more rainfall (Shanahan et al., 2008b).
 610 Proxy data generated from the BOS04-5B core suggest that progressively wetter conditions affected
 611 the catchment following ~73 ka (e.g., Gosling et al., 2022a; Shanahan et al., 2008b). Paleoclimate
 612 records based on the sediments of lakes Malawi (Tanzania), Bambili (Cameroon), Tanganyika
 613 (Tanzania/Democratic Republic of the Congo), Chew Bahir (Ethiopia) and Chala (Tanzania) (e.g.,
 614 Cohen et al., 2007; Foerster et al., 2022; Lézine et al., 2019; Scholz et al., 2007), and marine
 615 sediment core material from the West African margin (Figs. 1, 5) (e.g., Kinsley et al., 2022;
 616 Skonieczny et al., 2019) also pertain to a distinct regional-scale shift in hydro climate across tropical
 617 sub-Saharan Africa at this point in time (Fig. 5). Specifically, a shift characterized by a distinct
 618 moisture gradient favouring wetter conditions in the west of the continent relative to the east, which
 619 was further amplified during the last glacial termination (e.g., Baxter et al., 2023; Gosling et al., 2022a;
 620 Lupien et al., 2023), and were produced by a broader, regional-scale shift in hydroclimate across
 621 sub-Saharan Africa (Fig. 5). These records include deep drill cores from lakes Malawi (Tanzania),
 622 Bambili (Cameroon), Tanganyika (Tanzania/Democratic Republic of the Congo), Chew Bahir
 623 (Ethiopia) and Chala (Tanzania), and marine cores extracted from the West African margin (Figs. 1,
 624 5) (e.g., Kinsley et al., 2022; Skonieczny et al., 2019). Therefore, a coeval increase in the frequency
 625 and amplitude of Hg enrichment in Lake Bosumtwi, and associated rise in lake level, could indirectly
 626 reflect a regional-scale pronounced shifts in hydroclimate favouring wetter conditions in West across
 627 tropical sub-Saharan Africa.

Field Code Changed

Formatted: French (Switzerland)

Formatted: French (Switzerland)

Field Code Changed

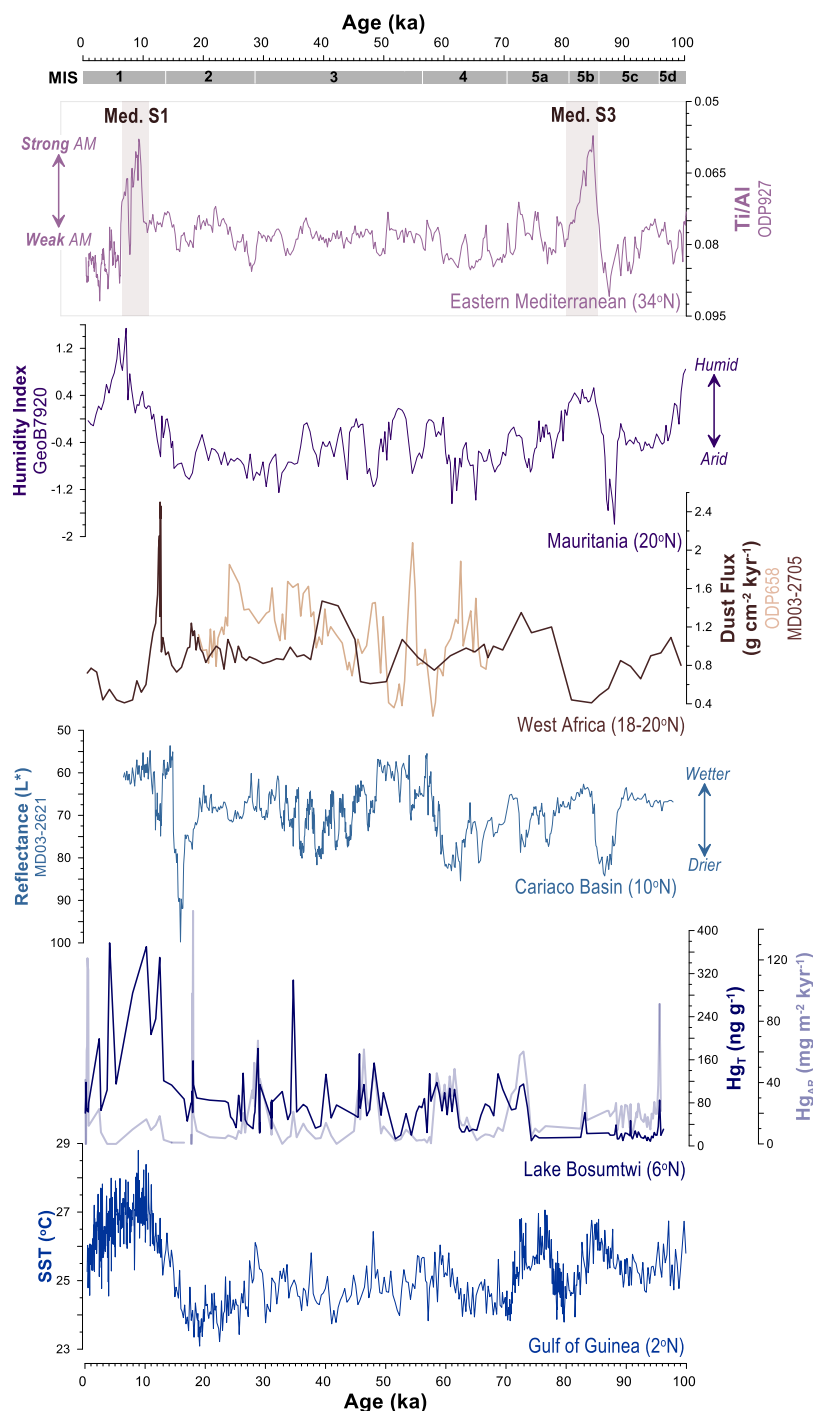


Figure 5: Records of total mercury (Hg_T) and mercury accumulation rate (Hg_{AR}) for Lake Bosumtwi generated by this study, compared with key paleoclimate records presented in order of latitude (physical locations shown in **Figure 1**), and known to be influenced by the WAM: sea-surface temperature (SST) reconstructed in core MD03-2707 from the Gulf of Guinea (Weldeab et al., 2007), sediment total reflectance (L^*) in marine core MD03-2621 from the Cariaco Basin, Venezuela, as a proxy for hydrological conditions anticipated in light of ITCZ oscillations over West Africa (Deplazes et al., 2013), dust fluxes recorded in cores ODP658 (Cap Blanc; Kinsley et al., 2022) and MD03-2705 (; Skonieczny et al., 2019), and a continental humidity index of core GeoB7920-2 (Mauritanian seamount; Tjallingii et al., 2008) – all from offshore Mauritania. Finally, Ti/Al recorded in core ODP 927 from the Eastern Mediterranean as a record of riverine (low Ti/Al) versus aeolian (high Ti/Al) North African inputs to the Mediterranean basin, and thus African monsoon intensity (Grant et al., 2022, 2017). Mediterranean sapropels one (Med. S1) and three (Med. S3) are marked by light brown bars (Grant et al., 2016). Light grey bars mark marine isotope stages (MIS) defined by the LR04 benthic marine isotope stack (Lisiecki and Raymo, 2005b).

Volcanic and wildfire activity are both linked to the Hg cycle. Although Lake Bosumtwi is located in close proximity to several highly productive volcanic regions, the resolution of BOS04-5B precludes our ability to examine Hg emissions with respect to single eruption events (**Fig. SF7**), and eruption record incompleteness coupled with time-transgressive changes in the global atmospheric Hg burden both complicate the ability to unambiguously correlate enhanced volcanic emissions to greater Hg deposition (**Fig. SF7**). Hydroclimate was also a key driver of changes in fire activity in tropical sub-Saharan Africa during the late Pleistocene (Moore et al. 2022). However, although wetter climatic conditions may be broadly associated with heightened fire activity due to associated increases in terrestrial biomass, recent work has shown that discrete changes in precipitation can elicit notably different fire responses between sites (e.g., Gosling et al., 2021; Karp et al., 2023). The influence of biomass burning on the Hg record presented here appears similarly complex; despite being a well-constrained factor in the Bosumtwi catchment, and evidence that wildfires are also a significant source of Hg, accounting for ~13% of natural Hg (re-)emissions to the modern atmosphere (Francisco López et al., 2022). Given that no clear relation is visible between Hg_T , Hg_{AR} , and two discrete macro- (Kiely, 2023) and micro- (Miller et al., 2016) charcoal profiles generated from the BOS04-5B core, we suggest that the effects of Hg emitted during wildfires also did not leave a clear imprint on Hg variability in this record (**Fig. SF8**).

Hydroclimate was a dominant driver of changes in fire activity in sub-Saharan Africa during the late Pleistocene. Wetter climatic conditions are typically associated with heightened fire activity due to associated increases in terrestrial biomass (e.g., Gosling et al., 2021; Moore et al., 2022), and wildfires are also a significant source of Hg, accounting for ~13% of natural Hg (re-)emissions to the modern atmosphere (Francisco López et al., 2022). The influence of biomass burning on the Hg record presented here is less clear; despite being a well-constrained factor in the Bosumtwi catchment. No clear correlation is visible between Hg_T , Hg_{AR} , and two discrete macro- (Kiely, 2023) and micro- (Miller et al., 2016) charcoal profiles generated from the BOS04-5B core, suggesting that the effects of Hg emitted during wildfires did not leave a clear imprint on Hg variability in this record (**Fig. S8**).

656

657 **5.6. Synthesis and conclusions**

658 ~~This study combines new sedimentary Hg data from Lake Bosumtwi, Ghana, with proxy data from~~
659 ~~archives across the African continent to explore whether hydroclimate has exerted a measurable~~
660 ~~effect on regional Hg cycling over the past ~96-kyr. This study seeks a better understanding of the~~
661 ~~impact that local, climate-driven environmental shifts may have on the terrestrial Hg cycle over~~
662 ~~multiple millennia.~~ The resolution of the BOS04-5B record (~0.6 kyr per sample) precludes a detailed
663 assessment of more recent (<0.2-kyr), anthropogenic-driven changes in local Hg cycling. However,
664 this record is well suited for a broader exploration of patterns and drivers of variability in sedimentary
665 Hg concentrations in Lake Bosumtwi during the late Pleistocene. Combining our results with existing
666 data reveals two possible drivers of variability in Hg_T and Hg_{AR} in Lake Bosumtwi on these timescales:
667 organic matter (host) availability, and local-scale changes in Hg input to the lake by precipitation (**Fig.**
668 **4**). Both are intrinsically coupled to the local hydroclimate by their link to the lake level, with higher
669 lake levels typically corresponding to wetter conditions in the catchment, and deposition of more
670 organic-rich sediments. **Figure 6** illustrates how selected environmental processes, under different
671 environmental conditions, may have interacted with these two drivers to control Hg burial in Lake
672 Bosumtwi between ~96 and 0 ka. Considered together, the evidence summarised in panels **(1)**, **(2)**,
673 and **(2a)** all suggest that rates of Hg drawdown in Lake Bosumtwi, and indeed the signals retained in
674 the sediment record, reflect changes in net Hg supply from the atmosphere.

675 Between ~96 and 73 ka (**Fig. 6, panel (1)**), generally arid conditions shifted the lake into a negative
676 water balance. Not only could this have reduced the net flux of Hg to the lake by wet deposition
677 (precipitation), but a negative water balance would also limit internal primary productivity and
678 preservation, and so render less organic material available to sequester any Hg present in the
679 system. Secondary dilution of Hg by detrital materials could have also lowered sedimentary Hg
680 concentrations, with elevated ~~elevated delivery of terrigenous matter to sediment delivery~~ to the
681 BOS04 site driven by exposure of the steep-sided crater walls during lake level lowering, and
682 heightened soil instability due to widespread recession of catchment vegetation. All would persist (if
683 not strengthen) during AI-1, and so could explain the lack of any measurable changes in Hg_T and
684 Hg_{AR} during this time.

685 Following an extended period of aridity, net supply of Hg to the basin would be increased by
686 precipitation following ~73 ka, which would simultaneously cause the lake to become deeper and
687 more stratified (**Fig. 6, panel (2)**). As the bottom waters became more oxygen-depleted, more
688 effective organic matter burial would simultaneously enhance Hg drawdown compared to detrital
689 mineral supply; with higher lake levels, vegetation growth, and soil stabilization preventing exposure
690 and erosion of the crater walls and soils surrounding the lake. Hence, this abrupt shift to humid (net-
691 positive precipitation-evaporation balance) conditions in the Bosumtwi catchment could plausibly have
692 driven an increase in sedimentary Hg concentrations and accumulation, by eliciting a pronounced rise
693 in lake level as well as increasing the atmospheric Hg flux.

694 The processes described in panel (2) would be amplified further between ~15 and 4 ka (**Fig. 6, panel**
695 **2a**). Corresponding to Bosumtwi sapropel unit 1, this unit marks a distinct humid period characterised
696 by anomalously high rainfall, and documented by proxy records across [tropical](#) sub-Saharan Africa
697 (Shanahan et al., 2015). For a closed lake system such as Lake Bosumtwi, these wetter conditions
698 would drive a sharp increase in lake depth, stratification, and scavenging in the water column – all of
699 which could favour heightened Hg drawdown to the sediment. 'Flattening' of the Hg-TOC relationship
700 during this interval also suggests that the Hg supply was (far) exceeded by the organic matter
701 availability (**Fig. S3a**), and so elevated Hg supply by precipitation could explain why Hg_T and Hg_{AR}
702 values are so unusually high (**Fig. 4a, 5**).

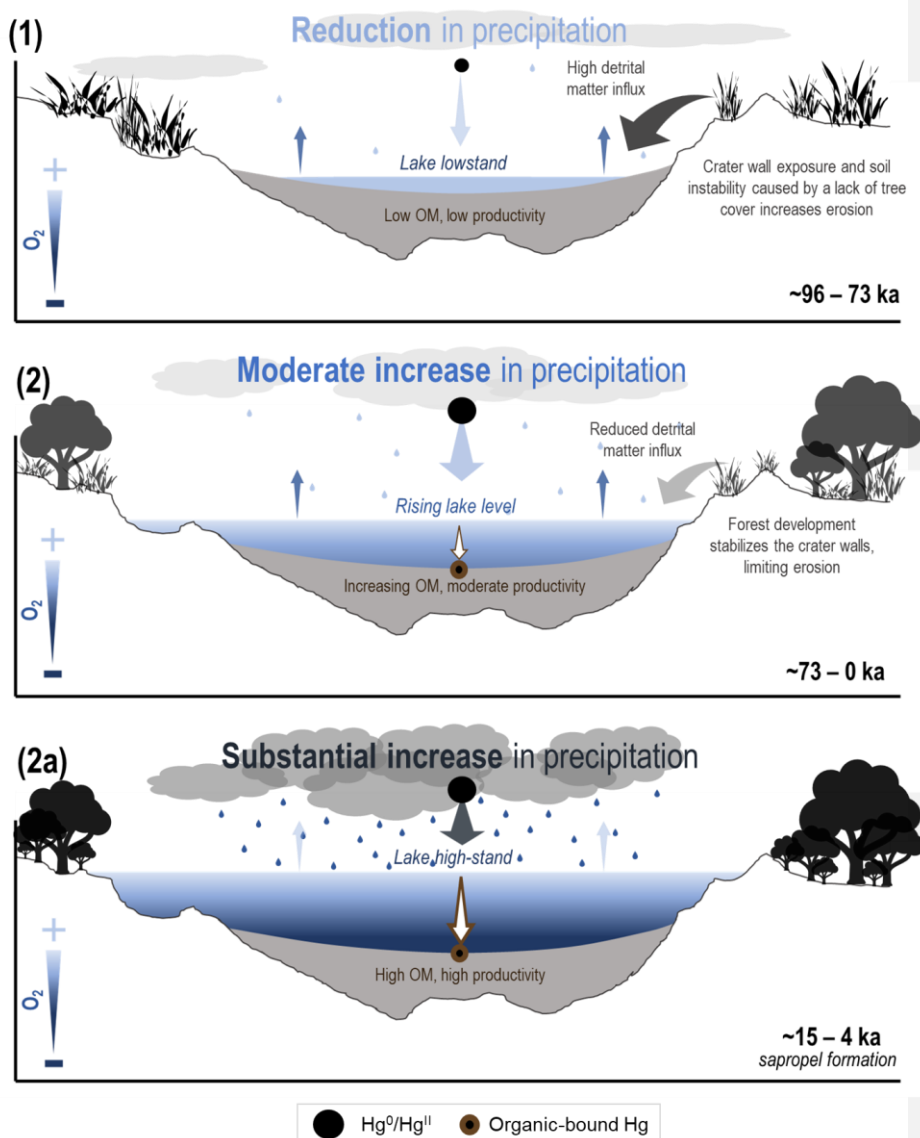


Figure 6: Schematic model depicting the processes that may control Hg flux, accumulation, and burial in Lake Bosumtwi under (1) arid (~93 – 73 ka), and (2) humid (~73 – 0 ka), environmental conditions. Panel (2a) depicts the very humid conditions that would be conducive to sapropel formation, such as those known to have occurred during the African Humid Period (~15 – 4 ka). Taken together, Hg fluxes increase during wet periods due to higher wet deposition directly to the lake relative to evasion, and/or by enhanced mobilization and transport of Hg from the catchment. Hg sequestration can also be enhanced by OM-scavenging in the water column, and increased lake stratification (anoxia at lake floor). The opposite occurs during dry intervals.

703 Future research should seek better constraints on how basin-specific variations in sediment
704 composition, lake structure, and water balance may influence how sedimentary Hg signals are
705 preserved and interpreted. This is because all could produce diverse, and perhaps contrasting, results
706 between lake systems. For example, results from Lake Bosumtwi suggest that lakes with smaller
707 watersheds, simple morphology, and minimal hydrological connectivity to the catchment could be
708 suitable targets to study catchment and intra-lake depositional processes over multiple millennia.
709 However, there are currently too few records covering these timescales to say this with certainty, and
710 not all closed lakes record measurable changes in Hg composition corresponding to changes in local
711 hydroclimate (Lent and Alexander, 1996; Pompeani et al., 2018). Organic matter/host phase
712 availability also appears to represent just one of several possible processes governing Hg burial in
713 lacustrine systems, given these systems are more readily affected by short-term changes in erosion,
714 nutrients, water balance, and catchment hydrology (Paine et al., 2024; Schütze et al., 2021).

715 Lake Bosumtwi is a small, morphologically simple lake. However, the complexity shown by its
716 sedimentary Hg record suggests that identical stratigraphic signals are unlikely to be recorded in
717 separate lakes, even if they are dominated by one common process, mechanism, and/or structure.
718 Exploring the importance of hydroclimate for Hg cycling relative to different catchment to lake area
719 ratios, hydrology (e.g., endorheic (closed) versus exoreic (open)), and/or catchment structures (e.g.,
720 forest versus savannah) would undoubtedly help to better resolve processes acting on single
721 lacustrine and terrestrial successions, but also identify the systems that may more sensitively record
722 major changes in Hg cycling. Provided the hydrological component of the Hg cycle can be isolated,
723 better characterization of the processes impacting lacustrine Hg cycling could also allow this element
724 to be used as a proxy for hydroclimatic change in terrestrial archives. For example, measurement of
725 sedimentary Hg isotopes in low-latitude and/or closed lakes could help quantify the contribution of Hg
726 to the sediment from precipitation or dry deposition, shedding new light on key biogeochemical
727 reaction pathways, processes (e.g., mass-independent fractionation (MIF)), and responses to
728 changing local hydrology across a range of timescales (e.g., Blum et al., 2014; Gao et al., 2023; Yin
729 et al., 2024).

730 This study provides new and valuable evidence for long-term interactions between terrestrial Hg
731 cycling and hydroclimate, and demonstrates that hydroclimate may be a key driver of Hg cycling in
732 tropical lakes over millennial-timescales. The sparse number of continuous, pre-industrial Hg records
733 currently available for sub-Saharan Africa have historically limited the ability to understand the extent
734 to which hydroclimate may drive long-term ($>10^2$ -year) variability in the Hg cycle (Schneider et al.,
735 2023), and subsequently how this relationship is represented in local and global ecosystem models
736 (Cooke et al., 2020; Obrist et al., 2018). Although this knowledge gap cannot be satisfied by a single
737 record, study of Lake Bosumtwi reinforces the value of these records for better characterization of the
738 Hg behaviour likely to be associated with projected future, monsoon-driven, hydroclimate variability
739 (Chang et al., 2022). In time, this could translate to better understanding of how the tropical Hg cycle
740 may respond to future, global-scale changes (Gustin et al., 2020; Schneider et al., 2023).

741

742 Competing Interests

743 The contact author has declared that none of the authors has any competing interest.

744 Acknowledgements

745 ARP, IMF, JF, and TAM acknowledge funding from European Research Council Consolidator Grant
746 V-ECHO (ERC-2018-COG-8187 17-V-ECHO). ARP thanks Christopher Scholz for provision of
747 sediment data, alongside James Bryson, Alex Dickson, and Erdem Idiz for insightful discussions in
748 early stages of manuscript preparation. Thanks also go to Stephen Wyatt (University of Oxford) for
749 analytical assistance throughout the study. All authors thank members of the International Continental
750 Scientific Drilling Program Lake Bosumtwi Drilling Project: for their efforts in extracting and producing
751 the sediment succession, and making the data available for scientific use.

752

753 References

- 754 [Åkerblom, S., Bishop, K., Björn, E., Lambertsson, L., Eriksson, T., Nilsson, M.B., 2013. Significant interaction](#)
755 [effects from sulfate deposition and climate on sulfur concentrations constitute major controls on](#)
756 [methylmercury production in peatlands. *Geochimica et Cosmochimica Acta* 102, 1–11.](#)
757 <https://doi.org/10.1016/j.gca.2012.10.025>
- 758 [Amos, H.M., Sonke, J.E., Obrist, D., Robins, N., Hagan, N., Horowitz, H.M., Mason, R.P., Witt, M., Hedgcock,](#)
759 [I.M., Corbitt, E.S., Sunderland, E.M., 2015. Observational and modeling constraints on global](#)
760 [anthropogenic enrichment of mercury. *Environmental Science and Technology* 49, 4036–4047.](#)
761 <https://doi.org/10.1021/es5058665>
- 762 [Armenteros, I., 2010. Diagenesis of Carbonates in Continental Settings. in: *Developments in Sedimentology*.](#)
763 [Elsevier, pp. 61–151. \[https://doi.org/10.1016/S0070-4571\\(09\\)06202-5\]\(https://doi.org/10.1016/S0070-4571\(09\)06202-5\)](#)
- 764 [Armstrong, E., Tallavaara, M., Hopcroft, P.O., Valdes, P.J., 2023. North African humid periods over the past](#)
765 [800,000 years. *Nat Commun* 14, 5549. <https://doi.org/10.1038/s41467-023-41219-4>](#)
- 766 [Baxter, A.J., Verschuren, D., Peterse, F., Miralles, D.G., Martin-Jones, C.M., Maitiuerdi, A., Van Der Meeren, T.,](#)
767 [Van Daele, M., Lane, C.S., Haug, G.H., Olago, D.O., Sinninghe Damsté, J.S., 2023. Reversed Holocene](#)
768 [temperature–moisture relationship in the Horn of Africa. *Nature* 620, 336–343.](#)
769 <https://doi.org/10.1038/s41586-023-06272-5>
- 770 [Benoit, J.M., Gilmour, C.C., Mason, R.P., Heyes, A., 1999. Sulfide controls on mercury speciation and](#)
771 [bioavailability to methylating bacteria in sediment pore water. *Environmental Science and Technology*](#)
772 [33, 1780. <https://doi.org/10.1021/es992007q>](#)
- 773 [Bertrand, S., Tjallingii, R., Kylander, M.E., Wilhelm, B., Roberts, S.J., Arnaud, F., Brown, E., Bindler, R., 2024.](#)
774 [Inorganic geochemistry of lake sediments: A review of analytical techniques and guidelines for data](#)
775 [interpretation. *Earth-Science Reviews* 249, 104639. <https://doi.org/10.1016/j.earscirev.2023.104639>](#)
- 776 [Biestler, H., Pérez-Rodríguez, M., Gilfedder, B.-S., Martínez Cortizas, A., Hermanns, Y.-M., 2018. Solar](#)
777 [irradiance and primary productivity controlled mercury accumulation in sediments of a remote lake in the](#)
778 [Southern Hemisphere during the past 4000 years: Primary productivity and mercury accumulation.](#)
779 [Limnol. Oceanogr. 63, 540–549. <https://doi.org/10.1002/lno.10647>](#)
- 780 [Bin, C., Xiaoru, W., Lee, F.S.C., 2001. Pyrolysis coupled with atomic absorption spectrometry for the](#)
781 [determination of mercury in Chinese medicinal materials. *Analytica Chimica Acta* 447, 161–169.](#)
782 [https://doi.org/10.1016/S0003-2670\(01\)01218-1](https://doi.org/10.1016/S0003-2670(01)01218-1)
- 783 [Bishop, K., Shanley, J.B., Riscassi, A., de Wit, H.A., Eklöf, K., Meng, B., Mitchell, C., Osterwalder, S., Schuster,](#)
784 [P.F., Webster, J., Zhu, W., 2020. Recent advances in understanding and measurement of mercury in](#)
785 [the environment: Terrestrial Hg cycling. *Science of the Total Environment* 721.](#)
786 <https://doi.org/10.1016/j.scitotenv.2020.137647>
- 787 [Blais, J.M., Kalff, J., 1995. The influence of lake morphometry on sediment focusing. *Limnol. Oceanogr.* 40, 582–](#)
788 [588. <https://doi.org/10.4319/lo.1995.40.3.0582>](#)
- 789 [Blum, J.D., Sherman, L.S., Johnson, M.W., 2014. Mercury Isotopes in Earth and Environmental Sciences. *Annu.*](#)
790 [Rev. Earth Planet. Sci. 42, 249–269. <https://doi.org/10.1146/annurev-earth-050212-124107>](#)
- 791 [Boamah, D., Koeberl, C., 2007. The Lake Bosumtwi impact structure in Ghana: A brief environmental](#)
792 [assessment and discussion of ecotourism potential. *Meteoritics and Planetary Science* 42, 561–567.](#)
793 <https://doi.org/10.1111/j.1945-5100.2007.tb01061.x>
- 794 [Bradley, R.S., Diaz, H.F., 2021. Late Quaternary Abrupt Climate Change in the Tropics and Sub-Tropics: The](#)
795 [Continental Signal of Tropical Hydroclimatic Events \(THEs\). *Reviews of Geophysics* 59,](#)
796 [e2020RG000732. <https://doi.org/10.1029/2020RG000732>](#)

- Branfireun, B.A., Cosio, C., Poulain, A.J., Riise, G., Bravo, A.G., 2020. Mercury cycling in freshwater systems - An updated conceptual model. *Science of the Total Environment* 745. <https://doi.org/10.1016/j.scitotenv.2020.140906>
- Bravo, A.G., Bouchet, S., Tolu, J., Björn, E., Mateos-Rivera, A., Bertilsson, S., 2017. Molecular composition of organic matter controls methylmercury formation in boreal lakes. *Nat Commun* 8, 14255. <https://doi.org/10.1038/ncomms14255>
- Brodie, C.R., Leng, M.J., Casford, J.S.L., Kendrick, C.P., Lloyd, J.M., Yongqiang, Z., Bird, M.I., 2011. Evidence for bias in C and N concentrations and $\delta^{13}\text{C}$ composition of terrestrial and aquatic organic materials due to pre-analysis acid preparation methods. *Chemical Geology* 282, 67–83. <https://doi.org/10.1016/j.chemgeo.2011.01.007>
- Brooks, K., Scholz, C.A., King, J.W., Peck, J., Overpeck, J.T., Russell, J.M., Amoako, P.Y.O., 2005. Late-Quaternary lowstands of lake Bosumtwi, Ghana: Evidence from high-resolution seismic-reflection and sediment-core data. *Palaeogeography, Palaeoclimatology, Palaeoecology* 216, 235–249. <https://doi.org/10.1016/j.palaeo.2004.10.005>
- Brumsack, H.J., 2006. The trace metal content of recent organic carbon-rich sediments: Implications for Cretaceous black shale formation. *Palaeogeography, Palaeoclimatology, Palaeoecology* 232, 344–361. <https://doi.org/10.1016/j.palaeo.2005.05.011>
- Chang, M., Liu, B., Wang, B., Martinez-Villalobos, C., Ren, G., Zhou, T., 2022. Understanding Future Increases in Precipitation Extremes in Global Land Monsoon Regions. *Journal of Climate* 35, 1839–1851. <https://doi.org/10.1175/JCLI-D-21-0409.1>
- Chede, B.S., Venancio, I.M., Figueiredo, T.S., Albuquerque, A.L.S., Silva-Filho, E.V., 2022. Mercury deposition in the western tropical South Atlantic during the last 70 ka. *Palaeogeography, Palaeoclimatology, Palaeoecology* 601, 111122. <https://doi.org/10.1016/j.palaeo.2022.111122>
- Cohen, A., Campisano, C., Arrowsmith, R., Asrat, A., Behrensmeyer, A.K., Deino, A., Feibel, C., Hill, A., Johnson, R., Kingston, J., Lamb, H., Lowenstein, T., Noren, A., Olago, D., Owen, R.B., Potts, R., Reed, K., Renaut, R., Schabitz, F., Tiercelin, J.-J., Trauth, M.H., Wynn, J., Ivory, S., Brady, K., O'Grady, R., Rodysill, J., Githiri, J., Russell, J., Foerster, V., Dommair, R., Rucina, S., Deocampo, D., Russell, J., Billingsley, A., Beck, C., Dorenbeck, G., Dullo, L., Feary, D., Garello, D., Gromig, R., Johnson, T., Junginger, A., Karanja, M., Kimburi, E., Mbuthia, A., McCartney, T., McNulty, E., Muiruri, V., Nambiro, E., Negash, E.W., Njagi, D., Wilson, J.N., Rabideaux, N., Raub, T., Sier, M.J., Smith, P., Urban, J., Warren, M., Yadeta, M., Yost, C., Zinaye, B., 2016. The Hominin Sites and Paleolakes Drilling Project: inferring the environmental context of human evolution from eastern African rift lake deposits. *Sci. Drill.* 21, 1–16. <https://doi.org/10.5194/sd-21-1-2016>
- Cohen, A.S., Campisano, C.J., Arrowsmith, J.R., Asrat, A., Beck, C.C., Behrensmeyer, A.K., Deino, A.L., Feibel, C.S., Foerster, V., Kingston, J.D., Lamb, H.F., Lowenstein, T.K., Lupien, R.L., Muiruri, V., Olago, D.O., Owen, R.B., Potts, R., Russell, J.M., Schabitz, F., Stone, J.R., Trauth, M.H., Yost, C.L., 2022. Reconstructing the Environmental Context of Human Origins in Eastern Africa Through Scientific Drilling. *Annu. Rev. Earth Planet. Sci.* 50, 451–476. <https://doi.org/10.1146/annurev-earth-031920-081947>
- Cohen, A.S., Stone, J.R., Beuning, K.R.M., Park, L.E., Reinthal, P.N., Dettman, D., Scholz, C.A., Johnson, T.C., King, J.W., Talbot, M.R., Brown, E.T., Ivory, S.J., 2007. Ecological consequences of early Late Pleistocene megadroughts in tropical Africa. *Proc. Natl. Acad. Sci. U.S.A.* 104, 16422–16427. <https://doi.org/10.1073/pnas.0703873104>
- Cooke, C.A., Martinez-Cortizas, A., Bindler, R., Sexauer Gustin, M., 2020. Environmental archives of atmospheric Hg deposition – A review. *Science of the Total Environment* 709, 134800. <https://doi.org/10.1016/j.scitotenv.2019.134800>
- Crocker, A.J., Naafs, B.D.A., Westerhold, T., James, R.H., Cooper, M.J., Röhl, U., Pancost, R.D., Xuan, C., Osborne, C.P., Beerling, D.J., Wilson, P.A., 2022. Astronomically controlled aridity in the Sahara since at least 11 million years ago. *Nat. Geosci.* 15, 671–676. <https://doi.org/10.1038/s41561-022-00990-7>
- deMenocal, P.B., 1995. Plio-Pleistocene African Climate. *Science* 270, 53–59. <https://doi.org/10.1126/science.270.5233.53>
- Deplazes, G., Lückge, A., Peterson, L.C., Timmermann, A., Hamann, Y., Hughen, K.A., Röhl, U., Laj, C., Cane, M.A., Sigman, D.M., Haug, G.H., 2013. Links between tropical rainfall and North Atlantic climate during the last glacial period. *Nature Geoscience* 6, 213–217. <https://doi.org/10.1038/ngeo1712>
- Edwards, B.A., Kushner, D.S., Outridge, P.M., Wang, F., 2021. Fifty years of volcanic mercury emission research: Knowledge gaps and future directions. *Science of the Total Environment* 757, 143800. <https://doi.org/10.1016/j.scitotenv.2020.143800>
- Engstrom, D.R., Rose, N.L., 2013. A whole-basin, mass-balance approach to paleolimnology. *J. Paleolimnol.* 49, 333–347. <https://doi.org/10.1007/s10933-012-9675-5>
- Fadina, O.A., Venancio, I.M., Belem, A., Silveira, C.S., Bertagnolli, D. de C., Silva-Filho, E.V., Albuquerque, A.L.S., 2019. Paleoclimatic controls on mercury deposition in northeast Brazil since the Last Interglacial. *Quaternary Science Reviews* 221, 105869. <https://doi.org/10.1016/j.quascirev.2019.105869>
- Figueiredo, T.S., Bergquist, B.A., Santos, T.P., Albuquerque, A.L.S., Silva-Filho, E.V., 2022. Relationship between glacial CO₂ drawdown and mercury cycling in the western South Atlantic: An isotopic insight. *Geology* 50, 3–7. <https://doi.org/10.1130/g49942.1>
- Foerster, V., Asrat, A., Bronk Ramsey, C., Brown, E.T., Chapot, M.S., Deino, A., Duesing, W., Grove, M., Hahn, A., Junginger, A., Kaboth-Bahr, S., Lane, C.S., Opitz, S., Noren, A., Roberts, H.M., Stockhecke, M.,

864 Tiedemann, R., Vidal, C.M., Vogelsang, R., Cohen, A.S., Lamb, H.F., Schaebitz, F., Trauth, M.H., 2022.
865 Pleistocene climate variability in eastern Africa influenced hominin evolution. *Nat. Geosci.* 15, 805–811.
866 <https://doi.org/10.1038/s41561-022-01032-y>

867 Francisco López, A., Heckenauer Barrón, E.G., Bello Bugallo, P.M., 2022. Contribution to understanding the
868 influence of fires on the mercury cycle: Systematic review, dynamic modelling and application to
869 sustainable hypothetical scenarios. *Environ Monit Assess* 194, 707. [https://doi.org/10.1007/s10661-022-](https://doi.org/10.1007/s10661-022-10208-3)
870 [10208-3](https://doi.org/10.1007/s10661-022-10208-3)

871 Frieling, J., Mather, T.A., März, C., Jenkyns, H.C., Hennekam, R., Reichart, G.-J., Slomp, C.P., Van Helmond,
872 N.A.G.M., 2023. Effects of redox variability and early diagenesis on marine sedimentary Hg records.
873 *Geochimica et Cosmochimica Acta* S0016703723001850. <https://doi.org/10.1016/j.gca.2023.04.015>

874 Gao, X., Yuan, W., Chen, J., Huang, F., Wang, Z., Gong, Y., Zhang, Y., Liu, Y., Zhang, T., Zheng, W., 2023.
875 Tracing the source and transport of Hg during pedogenesis in strongly weathered tropical soil using Hg
876 isotopes. *Geochimica et Cosmochimica Acta* 361, 101–112. <https://doi.org/10.1016/j.gca.2023.10.009>

877 Gehrke, G.E., Blum, J.D., Meyers, P.A., 2009. The geochemical behavior and isotopic composition of Hg in a
878 mid-Pleistocene western Mediterranean sapropel. *Geochimica et Cosmochimica Acta* 73, 1651–1665.
879 <https://doi.org/10.1016/j.gca.2008.12.012>

880 Gosling, W.D., McMichael, C.N.H., Groenwoud, Z., Roding, E., Miller, C.S., Julier, A.C.M., 2021. Preliminary
881 evidence for green, brown and black worlds in tropical western Africa during the Middle and Late
882 Pleistocene. *Palaeoecology of Africa* 35, 13–25. <https://doi.org/10.1201/9781003162766>

883 Gosling, W.D., Miller, C.S., Shanahan, T.M., Holden, P.B., Overpeck, J.T., van Langevelde, Frank., 2022a. A
884 stronger role for long-term moisture change than for CO₂ in determining tropical woody vegetation
885 change. *Science* 376, 653–656. <https://doi.org/10.1126/science.abg4618>

886 Gosling, W.D., Scerri, E.M.L., Kaboth-Bahr, S., 2022b. The climate and vegetation backdrop to hominin evolution
887 in Africa. *Philosophical Transactions of the Royal Society B: Biological Sciences* 377.
888 <https://doi.org/10.1098/rstb.2020.0483>

889 Grant, K.M., Amarathunga, U., Amies, J.D., Hu, P., Qian, Y., Penny, T., Rodriguez-Sanz, L., Zhao, X., Heslop,
890 D., Liebrand, D., Hennekam, R., Westerhold, T., Gilmore, S., Lourens, L.J., Roberts, A.P., Rohling, E.J.,
891 2022. Organic carbon burial in Mediterranean sapropels intensified during Green Sahara Periods since
892 3.2 Myr ago. *Commun Earth Environ* 3, 11. <https://doi.org/10.1038/s43247-021-00339-9>

893 Grant, K.M., Grimm, E.C., Mikolajewicz, U., Marino, G., Ziegler, M., Rohling, E.J., 2016. The timing of
894 Mediterranean sapropel deposition relative to insolation, sea-level and African monsoon changes.
895 *Quaternary Science Reviews* 140, 125–141. <https://doi.org/10.1016/j.quascirev.2016.03.026>

896 Grant, K.M., Rohling, E.J., Westerhold, T., Zabel, M., Heslop, D., Konijnendijk, T., Lourens, L., 2017. A 3 million
897 year index for North African humidity/aridity and the implication of potential pan-African humid periods.
898 *Quaternary Science Reviews* 171, 100–118. <https://doi.org/10.1016/j.quascirev.2017.07.005>

899 Grygar, T.M., Mach, K., Martinez, M., 2019. Checklist for the use of potassium concentrations in siliciclastic
900 sediments as paleoenvironmental archives. *Sedimentary Geology* 382, 75–84.
901 <https://doi.org/10.1016/j.sedgeo.2019.01.010>

902 Guédron, S., Ledru, M.P., Escobar-Torrez, K., Develle, A.L., Brisset, E., 2018. Enhanced mercury deposition by
903 Amazonian orographic precipitation: Evidence from high-elevation Holocene records of the Lake
904 Titicaca region (Bolivia). *Palaeogeography, Palaeoclimatology, Palaeoecology* 511, 577–587.
905 <https://doi.org/10.1016/j.palaeo.2018.09.023>

906 Gulati, R.D., Zadereev, E.S., Degermendzhi, A.G. (Eds.), 2017. *Ecology of Meromictic Lakes, Ecological Studies*.
907 Springer International Publishing, Cham. <https://doi.org/10.1007/978-3-319-49143-1>

908 Gustin, M.S., Bank, M.S., Bishop, K., Bowman, K., Branfireun, B., Chételat, J., Eckley, C.S., Hammerschmidt,
909 C.R., Lamborg, C., Lyman, S., Martínez-Cortizas, A., Sommar, J., Tsui, M.T.-K., Zhang, T., 2020.
910 Mercury biogeochemical cycling: A synthesis of recent scientific advances. *Science of The Total*
911 *Environment* 737, 139619. <https://doi.org/10.1016/j.scitotenv.2020.139619>

912 Ha, J., Zhao, X., Yu, R., Barkay, T., Yee, N., 2017. Hg(II) reduction by siderite (FeCO₃). *Applied Geochemistry*
913 78, 211–218. <https://doi.org/10.1016/j.apgeochem.2016.12.017>

914 Hammer, Ø., Harper, D.A.T., Ryan, P.D., 2001. PAST: Paleontological statistics software package for education
915 and data analysis. *Palaeontologia Electronica* 4, 9.

916 Han, S., Obraztsova, A., Pretto, P., Deheyn, D.D., Gieskes, J., Tebo, B.M., 2008. Sulfide and iron control on
917 mercury speciation in anoxic estuarine sediment slurries. *Marine Chemistry* 111, 214–220.
918 <https://doi.org/10.1016/j.marchem.2008.05.002>

919 Hermanns, Y.M., Biester, H., 2013. A 17,300-year record of mercury accumulation in a pristine lake in southern
920 Chile. *Journal of Paleolimnology* 49, 547–561. <https://doi.org/10.1007/s10933-012-9668-4>

921 Hermanns, Y.M., Cortizas, A.M., Arz, H., Stein, R., Biester, H., 2013. Untangling the influence of in-lake
922 productivity and terrestrial organic matter flux on 4,250 years of mercury accumulation in Lake Hambro,
923 Southern Chile. *Journal of Paleolimnology* 49, 563–573. <https://doi.org/10.1007/s10933-012-9657-7>

924 Hernández, A., Martín-Puertas, C., Moffa-Sánchez, P., Moreno-Chamarro, E., Ortega, P., Blockley, S., Cobb, K.,
925 Comas-Bru, L., Giralt, S., Goosse, H., Luterbacher, J., Martrat, B., Muscheler, R., Parnell, A., Pla-
926 Rabes, S., Sjolte, J., Scaife, A., Swingedouw, D., Wise, E., Xu, G., 2020. Modes of climate variability:
927 Synthesis and review of proxy-based reconstructions through the Holocene. *Earth-Science Reviews*
928 209, 103286. <https://doi.org/10.1016/j.earscirev.2020.103286>

Hsu-Kim, H., Kucharczyk, K.H., Zhang, T., Deshusses, M.A., 2013. Mechanisms Regulating Mercury Bioavailability for Methylating Microorganisms in the Aquatic Environment: A Critical Review. *Environ. Sci. Technol.* 47, 2441–2456. <https://doi.org/10.1021/es304370g>

Jenkyns, H.C., 1988. The Early Toarcian (Jurassic) Anoxic Event. *American Journal of Science*.

Jenkyns, H.C., Weedon, G.P., 2013. Chemostratigraphy (CaCO₃, TOC, $\delta^{13}\text{C}_{\text{org}}$) of Sinemurian (Lower Jurassic) black shales from the Wessex Basin, Dorset and palaeoenvironmental implications. *nos 46*, 1–21. <https://doi.org/10.1127/0078-0421/2013/0029>

Jeon, B., Scirio, A., Cizdziel, J.V., Chen, J., Black, O., Wallace, D.J., Zhou, Y., Lepak, R.F., Hurley, J.P., 2020. Historical deposition of trace metals in a marine sapropel from Mangrove Lake, Bermuda with emphasis on mercury, lead, and their isotopic composition. *J. Soils Sediments* 20, 2266–2276. <https://doi.org/10.1007/s11368-020-02567-6>

Jones, W.B., Bacon, M., Hastings, D.A., 1981. The Lake Bosumtwi impact crater, Ghana. *Geological Society of America Bulletin* 92, 342–349. [https://doi.org/10.1130/0016-7606\(1981\)92<342:TLBICG>2.0.CO;2](https://doi.org/10.1130/0016-7606(1981)92<342:TLBICG>2.0.CO;2)

Jourdan, F., Renne, P.R., Reimold, W.U., 2009. An appraisal of the ages of terrestrial impact structures. *Earth and Planetary Science Letters* 286, 1–13. <https://doi.org/10.1016/j.epsl.2009.07.009>

Kaboth-Bahr, S., Gosling, W.D., Vogelsang, R., Bahr, A., Scerri, E.M.L., 2021. Paleo-ENSO influence on African environments and early modern humans. *Proceedings of the National Academy of Science* 118, 1–6. <https://doi.org/10.1073/pnas.2018277118>

Karp, A.T., Uno, K.T., Berke, M.A., Russell, J.M., Scholz, C.A., Marlon, J.R., Faith, J.T., Staver, A.C., 2023. Nonlinear rainfall effects on savanna fire activity across the African Humid Period. *Quaternary Science Reviews* 304, 107994. <https://doi.org/10.1016/j.quascirev.2023.107994>

Kiely, R., 2023. A 50,000-year reconstruction of West African fire history (MSc Thesis). University of Amsterdam, Amsterdam.

Kinsley, C.W., Bradtmiller, L.I., McGee, D., Galgay, M., Stuut, J.B., Tjallingii, R., Winckler, G., DeMenocal, P.B., 2022. Orbital and Millennial-Scale Variability in Northwest African Dust Emissions Over the Past 67,000 years. *Paleoceanography and Paleoclimatology* 37, 1–22. <https://doi.org/10.1029/2020PA004137>

Koeberl, C., Milkereit, B., Overpeck, J.T., Scholz, C.A., Amoako, P.Y.O., Boamah, D., Danuor, S.K., Karp, T., Kueck, J., Hecky, R.E., King, J.W., Peack, J.A., 2007. An international and multidisciplinary drilling project into a young complex impact structure: The 2004 ICDP Bosumtwi Crater Drilling Project - An overview. *Meteoritics and Planetary Science* 42, 483–511. <https://doi.org/10.1111/j.1945-5100.2007.tb01057.x>

Koeberl, C., Peck, J., King, J., Milkereit, B., Overpeck, J., Scholz, C., 2005. The ICDP lake Bosumtwi drilling project: A first report. *Scientific Drilling* 1, 23–27. <https://doi.org/10.2204/iodp.sd.1.04.2005>

Kuechler, R.R., Schefuß, E., Beckmann, B., Dupont, L., Wefer, G., 2013. NW African hydrology and vegetation during the Last Glacial cycle reflected in plant-wax-specific hydrogen and carbon isotopes. *Quaternary Science Reviews* 82, 56–67. <https://doi.org/10.1016/j.quascirev.2013.10.013>

Kuss, J., Zülcke, C., Pohl, C., Schneider, B., 2011. Atlantic mercury emission determined from continuous analysis of the elemental mercury sea-air concentration difference within transects between 50°N and 50°S. *Global Biogeochem. Cycles* 25. <https://doi.org/10.1029/2010GB003998>

Larrasoana, J.C., Roberts, A.P., Rohling, E.J., 2013. Dynamics of Green Sahara Periods and Their Role in Hominin Evolution. *PLoS ONE* 8. <https://doi.org/10.1371/journal.pone.0076514>

Laskar, J., Robutel, P., Joutel, F., Gastineau, M., Correia, A.C.M., Levrard, B., 2004. A long-term numerical solution for the insolation quantities of the Earth. *Astronomy and Astrophysics* 428, 261–285. <https://doi.org/10.1051/0004-6361:20041335>

Leiva González, J., Díaz-Robles, L.A., Cereceda-Balic, F., Pino-Cortés, E., Campos, V., 2022. Atmospheric Modelling of Mercury in the Southern Hemisphere and Future Research Needs: A Review. *Atmosphere* 13, 1226. <https://doi.org/10.3390/atmos13081226>

Lent, R.M., Alexander, C.R., 1996. Mercury accumulation in Devils Lake, north Dakota - effects of environmental variation in closed-basin lakes on mercury chronologies. *Water, Air, & Soil Pollution* 98, 275–296.

Lézine, A.-M., Izumi, K., Kageyama, M., Achoundong, G., 2019. A 90,000-year record of Afromontane forest responses to climate change. *Science* 363, 177–181. <https://doi.org/10.1126/science.aav6821>

Li, F., Ma, C., Zhang, P., 2020. Mercury Deposition, Climate Change and Anthropogenic Activities: A Review. *Frontiers in Earth Science* 8, 316. <https://doi.org/10.3389/feart.2020.00316>

Lisiecki, L.E., Raymo, M.E., 2005a. A Pliocene-Pleistocene stack of 57 globally distributed benthic $\delta^{18}\text{O}$ records. *Paleoceanography* 20, 1–17. <https://doi.org/10.1029/2004PA001071>

Lisiecki, L.E., Raymo, M.E., 2005b. A Pliocene-Pleistocene stack of 57 globally distributed benthic $\delta^{18}\text{O}$ records. *Paleoceanography* 20, 1–17. <https://doi.org/10.1029/2004PA001071>

Liu, M., Zhang, Q., Maavara, T., Liu, S., Wang, X., Raymond, P.A., 2021. Rivers as the largest source of mercury to coastal oceans worldwide. *Nature Geoscience* 14, 672–677. <https://doi.org/10.1038/s41561-021-00793-2>

Lupien, R., Uno, K., Rose, C., deRoberts, N., Hazan, C., De Menocal, P., Polissar, P., 2023. Low-frequency orbital variations controlled climatic and environmental cycles, amplitudes, and trends in northeast Africa during the Plio-Pleistocene. *Commun Earth Environ* 4, 360. <https://doi.org/10.1038/s43247-023-01034-7>

Lyman, S.N., Cheng, I., Gratz, L.E., Weiss-Penzias, P., Zhang, L., 2020. An updated review of atmospheric mercury. *Science of the Total Environment* 707, 135575. <https://doi.org/10.1016/j.scitotenv.2019.135575>

- Machado, W., Sanders, C.J., Santos, I.R., Sanders, L.M., Silva-Filho, E.V., Luiz-Silva, W., 2016. Mercury dilution by autochthonous organic matter in a fertilized mangrove wetland. *Environmental Pollution* 213, 30–35. <https://doi.org/10.1016/j.envpol.2016.02.002>
- Mason, R.P., Laporte, J.M., Andres, S., 2000. Factors controlling the bioaccumulation of mercury, methylmercury, arsenic, selenium, and cadmium by freshwater invertebrates and fish. *Archives of Environmental Contamination and Toxicology* 38, 283–297. <https://doi.org/10.1007/s002449910038>
- McKay, N.P., 2012. A multidisciplinary approach to late Quaternary paleoclimatology with an emphasis on sub-saharan West Africa and the last interglacial period (PhD Thesis). University of Arizona, Arizona.
- Menviel, L., Govin, A., Avenas, A., Meissner, K.J., Grant, K.M., Tzedakis, P.C., 2021. Drivers of the evolution and amplitude of African Humid Periods. *Commun Earth Environ* 2, 237. <https://doi.org/10.1038/s43247-021-00309-1>
- Miller, C.S., Gosling, W.D., 2014. Quaternary forest associations in lowland tropical West Africa. *Quaternary Science Reviews* 84, 7–25. <https://doi.org/10.1016/j.quascirev.2013.10.027>
- Miller, C.S., Gosling, W.D., Kemp, D.B., Coe, A.L., Gilmour, I., 2016. Drivers of ecosystem and climate change in tropical West Africa over the past ~540 000 years. *Journal of Quaternary Science* 31, 671–677. <https://doi.org/10.1002/jqs.2893>
- Nalbant, J., Schneider, L., Hamilton, R., Connor, S., Biester, H., Stuart-Williams, H., Bergal-Kuvikas, O., Jacobsen, G., Stevenson, J., 2023. Fire, volcanism and climate change: the main factors controlling mercury (Hg) accumulation rates in Tropical Lake Lantao, Sulawesi, Indonesia (~16,500–540 cal yr BP). *Front. Environ. Chem.* 4, 1241176. <https://doi.org/10.3389/fenvc.2023.1241176>
- Nicholson, S.E., 2013. The West African Sahel: A Review of Recent Studies on the Rainfall Regime and Its Interannual Variability. *ISRN Meteorology* 2013, 1–32. <https://doi.org/10.1155/2013/453521>
- Obriest, D., Kirk, J.L., Zhang, L., Sunderland, E.M., Jiskra, M., Selin, N.E., 2018. A review of global environmental mercury processes in response to human and natural perturbations: Changes of emissions, climate, and land use. *Ambio* 47, 116–140. <https://doi.org/10.1007/s13280-017-1004-9>
- O'Mara, N.A., Skonieczny, C., McGee, D., Winckler, G., Bory, A.J.-M., Bradtmiller, L.I., Malaizé, B., Polissar, P.J., 2022. Pleistocene drivers of Northwest African hydroclimate and vegetation. *Nat Commun* 13, 3552. <https://doi.org/10.1038/s41467-022-31120-x>
- Outridge, P.M., Stern, G.A., Hamilton, P.B., Sanei, H., 2019. Algal scavenging of mercury in preindustrial Arctic lakes. *Limnol Oceanogr* 64, 1558–1571. <https://doi.org/10.1002/lno.11135>
- Outridge, Sanei, H., Stern, G.A., Hamilton, P.B., Goodarzi, F., 2007. Evidence for Control of Mercury Accumulation Rates in Canadian High Arctic Lake Sediments by Variations of Aquatic Primary Productivity. *Environ. Sci. Technol.* 41, 5259–5265. <https://doi.org/10.1021/es070408x>
- Paine, A.R., Fendley, I.M., Frieling, J., Mather, T.A., Lacey, J.H., Wagner, B., Robinson, S.A., Pyle, D.M., Francke, A., Them II, T.R., Panagiotopoulos, K., 2024. Mercury records covering the past 90 000 years from lakes Prespa and Ohrid, SE Europe. *Biogeosciences* 21, 531–556. <https://doi.org/10.5194/bg-21-531-2024>
- Pan, J., Zhong, W., Wei, Z., Ouyang, J., Shang, S., Ye, S., Chen, Y., Xue, J., Tang, X., 2020. A 15,400-year record of natural and anthropogenic input of mercury (Hg) in a sub-alpine lacustrine sediment succession from the western Nanling Mountains, South China. *Environmental Science and Pollution Research* 27, 20478–20489. <https://doi.org/10.1007/s11356-020-08421-z>
- Pausata, F.S.R., Gaetani, M., Messori, G., Berg, A., Maia de Souza, D., Sage, R.F., deMenocal, P.B., 2020. The Greening of the Sahara: Past Changes and Future Implications. *One Earth* 2, 235–250. <https://doi.org/10.1016/j.oneear.2020.03.002>
- Peck, J.A., Green, R.R., Shanahan, T., King, J.W., Overpeck, J.T., Scholz, C.A., 2004. A magnetic mineral record of Late Quaternary tropical climate variability from Lake Bosumtwi, Ghana. *Palaeogeography, Palaeoclimatology, Palaeoecology* 215, 37–57. <https://doi.org/10.1016/j.palaeo.2004.08.003>
- Pérez-Rodríguez, M., Margalef, O., Corella, J.P., Saiz-Lopez, A., Pla-Rabes, S., Giral, S., Cortizas, A.M., 2018. The role of climate: 71 ka of atmospheric mercury deposition in the southern hemisphere recorded by Rano Aroi Mire, Easter Island (Chile). *Geosciences (Switzerland)* 8. <https://doi.org/10.3390/geosciences8100374>
- Pilla, R.M., Williamson, C.E., Adamovich, B.V., Adrian, R., Anneville, O., Chandra, S., Colom-Montero, W., Devlin, S.P., Dix, M.A., Dokulil, M.T., Gaiser, E.E., Girdner, S.F., Hambright, K.D., Hamilton, D.P., Havens, K., Hessen, D.O., Higgins, S.N., Huttula, T.H., Huuskonen, H., Isles, P.D.F., Joehnk, K.D., Jones, I.D., Keller, W.B., Knoll, L.B., Korhonen, J., Kraemer, B.M., Leavitt, P.R., Lepori, F., Luger, M.S., Maberly, S.C., Melack, J.M., Melles, S.J., Müller-Navarra, D.C., Pierson, D.C., Pislegina, H.V., Plisnier, P.-D., Richardson, D.C., Rimmer, A., Rogora, M., Rusak, J.A., Sadro, S., Salmasso, N., Saros, J.E., Saulnier-Talbot, É., Schindler, D.E., Schmid, M., Shimaraeva, S.V., Silow, E.A., Sitoki, L.M., Sommaruga, R., Straile, D., Strock, K.E., Thiery, W., Timofeyev, M.A., Verburg, P., Vinebrooke, R.D., Weyhenmeyer, G.A., Zadereev, E., 2020. Deeper waters are changing less consistently than surface waters in a global analysis of 102 lakes. *Sci Rep* 10, 20514. <https://doi.org/10.1038/s41598-020-76873-x>
- Pompeani, D.P., Cooke, C.A., Abbott, M.B., Drevnick, P.E., 2018. Climate, Fire, and Vegetation Mediate Mercury Delivery to Midlatitude Lakes over the Holocene. *Environmental Science and Technology* 52, 8157–8164. <https://doi.org/10.1021/acs.est.8b01523>
- Ravichandran, M., 2004. Interactions between mercury and dissolved organic matter - A review. *Chemosphere* 55, 319–331. <https://doi.org/10.1016/j.chemosphere.2003.11.011>

Russell, J., Talbot, M.R., Haskell, B.J., 2003. Mid-holocene climate change in Lake Bosumtwi, Ghana. *Quaternary Research* 60, 133–141. [https://doi.org/10.1016/S0033-5894\(03\)00065-6](https://doi.org/10.1016/S0033-5894(03)00065-6)

Sanei, H., Grasby, S., Beauchamp, B., 2012. Latest Permian mercury anomalies. *Geology* 40, 63–66.

Schneider, L., Cooke, C.A., Stansell, N.D., Haberle, S.G., 2020. Effects of climate variability on mercury deposition during the Older Dryas and Younger Dryas in the Venezuelan Andes. *Journal of Paleolimnology* 63, 211–224. <https://doi.org/10.1007/s10933-020-00111-7>

Schneider, L., Fisher, J.A., Diéquez, M.C., Fostier, A.-H., Guimaraes, J.R.D., Leaner, J.J., Mason, R., 2023. A synthesis of mercury research in the Southern Hemisphere, part 1: Natural processes. *Ambio* 52, 897–917. <https://doi.org/10.1007/s13280-023-01832-5>

Scholz, C.A., Johnson, T.C., Cohen, A.S., King, J.W., Peck, J.A., Overpeck, J.T., Talbot, M.R., Brown, E.T., Kalindekafe, L., Amoako, P.Y.O., Lyons, R.P., Shanahan, T.M., Castañeda, I.S., Heil, C.W., Forman, S.L., McHargue, L.R., Beuning, K.R., Gomez, J., Pierson, J., 2007. East African megadroughts between 135 and 75 thousand years ago and bearing on early-modern human origins. *Proceedings of the National Academy of Sciences of the United States of America* 104, 16416–16421. <https://doi.org/10.1073/pnas.0703874104>

Schultze, M., Boehrer, B., Wendt-Potthoff, K., Katsev, S., Brown, E.T., 2017. Chemical Setting and Biogeochemical Reactions in Meromictic Lakes, in: *Ecology of Meromictic Lakes*. Springer, pp. 35–61.

Schütze, M., Gatz, P., Gilfedder, B., Biester, H., 2021. Why productive lakes are larger mercury sedimentary sinks than oligotrophic brown water lakes. *Limnol Oceanogr* 66, 1316–1332. <https://doi.org/10.1002/lno.11684>

Schütze, M., Tserendorj, G., Pérez-Rodríguez, M., Rösch, M., Biester, H., 2018. Prediction of Holocene mercury accumulation trends by combining palynological and geochemical records of lake sediments (Black Forest, Germany). *Geosciences (Switzerland)* 8. <https://doi.org/10.3390/geosciences8100358>

Sebag, D., Garcin, Y., Adatte, T., Deschamps, P., Ménot, G., Verrecchia, E.P., 2018. Correction for the siderite effect on Rock-Eval parameters: Application to the sediments of Lake Barombi (southwest Cameroon). *Organic Geochemistry* 123, 126–135. <https://doi.org/10.1016/j.orggeochem.2018.05.010>

Segato, D., Saiz-Lopez, A., Mahajan, A.S., Wang, F., Corella, J.P., Cuevas, C.A., Erhardt, T., Jensen, C.M., Zeppenfeld, C., Kjær, H.A., Turetta, C., Cairns, W.R.L., Barbante, C., Spolaor, A., 2023. Arctic mercury flux increased through the Last Glacial Termination with a warming climate. *Nat. Geosci.* 16, 439–445. <https://doi.org/10.1038/s41561-023-01172-9>

Selin, N.E., 2009. Global biogeochemical cycling of mercury: a review. *Annual Review of Environmental Resources* 34, 43–63.

Shanahan, T.M., Beck, J.W., Overpeck, J.T., McKay, N.P., Pigati, J.S., Peck, J.A., Scholz, C.A., Heil, C.W., King, J., 2012. Late Quaternary sedimentological and climate changes at Lake Bosumtwi Ghana: New constraints from laminae analysis and radiocarbon age modeling. *Palaeogeography, Palaeoclimatology, Palaeoecology* 361–362, 49–60. <https://doi.org/10.1016/j.palaeo.2012.08.001>

Shanahan, T.M., McKay, N.P., Hughen, K.A., Overpeck, J.T., Otto-Bliesner, B., Heil, C.W., King, J., Scholz, C.A., Peck, J., 2015. The time-transgressive termination of the African humid period. *Nature Geoscience* 8, 140–144. <https://doi.org/10.1038/ngeo2329>

Shanahan, T.M., Overpeck, J.T., Anchukaitis, K.J., Beck, J.W., Cole, J.E., Dettman, D.L., Peck, J.A., Scholz, C.A., King, J.W., 2009. Atlantic forcing of persistent drought in West Africa. *Science* 324, 377–380. <https://doi.org/10.1126/science.1166352>

Shanahan, T.M., Overpeck, J.T., Beck, J.W., Wheeler, C.W., Peck, J.A., King, J.W., Scholz, C.A., 2008a. The formation of biogeochemical laminations in Lake Bosumtwi, Ghana, and their usefulness as indicators of past environmental changes. *Journal of Paleolimnology* 40, 339–355. <https://doi.org/10.1007/s10933-007-9164-4>

Shanahan, T.M., Overpeck, J.T., Scholz, C.A., Beck, J.W., Peck, J., King, J.W., 2008b. Abrupt changes in the water balance of tropical West Africa during the late Quaternary. *J. Geophys. Res.* 113, D12108. <https://doi.org/10.1029/2007JD009320>

Shanahan, T.M., Overpeck, J.T., Sharp, W.E., Scholz, C.A., Arko, J.A., 2007. Simulating the response of a closed-basin lake to recent climate changes in tropical West Africa (Lake Bosumtwi, Ghana). *Hydrological Processes* 21, 1678–1691. <https://doi.org/10.1002/hyp.6359>

Shanahan, T.M., Overpeck, J.T., Wheeler, C.W., Beck, J.W., Pigati, J.S., Talbot, M.R., Scholz, C.A., Peck, J., King, J.W., 2006. Paleoclimatic variations in West Africa from a record of late Pleistocene and Holocene lake level stands of Lake Bosumtwi, Ghana. *Palaeogeography, Palaeoclimatology, Palaeoecology* 242, 287–302. <https://doi.org/10.1016/j.palaeo.2006.06.007>

Shanahan, T.M., Peck, J.A., McKay, N., Heil, C.W., King, J., Forman, S.L., Hoffmann, D.L., Richards, D.A., Overpeck, J.T., Scholz, C., 2013. Age models for long lacustrine sediment records using multiple dating approaches - An example from Lake Bosumtwi, Ghana. *Quaternary Geochronology* 15, 47–60. <https://doi.org/10.1016/j.quageo.2012.12.001>

Shen, J., Feng, Q., Algeo, T.J., Liu, Jinling, Zhou, C., Wei, W., Liu, Jiangsi, Them, T.R., Gill, B.C., Chen, J., 2020. Sedimentary host phases of mercury (Hg) and implications for use of Hg as a volcanic proxy. *Earth and Planetary Science Letters* 543, 116333. <https://doi.org/10.1016/j.epsl.2020.116333>

Skonieczny, C., McGee, D., Winckler, G., Bory, A., Bradtmiller, L.I., Kinsley, C.W., Polissar, P.J., De Pol-Holz, R., Rossignol, L., Malaizé, B., 2019. Monsoon-driven Saharan dust variability over the past 240,000 years. *Science Advances* 5, 1–9. <https://doi.org/10.1126/sciadv.aav1887>

- Soerensen, A.L., Mason, R.P., Balcom, P.H., Jacob, D.J., Zhang, Y., Kuss, J., Sunderland, E.M., 2014. Elemental Mercury Concentrations and Fluxes in the Tropical Atmosphere and Ocean. *Environ. Sci. Technol.* 48, 11312–11319. <https://doi.org/10.1021/es503109p>
- Sprovieri, F., Pirrone, N., Bencardino, M., D'Amore, F., Angot, H., Barbante, C., Brunke, E.-G., Arcega-Cabrera, F., Cairns, W., Comero, S., Diéquez, M. del C., Dommergue, A., Ebinghaus, R., Feng, X.B., Fu, X., Garcia, P.E., Gawlik, B.M., Hageström, U., Hansson, K., Horvat, M., Kotnik, J., Labuschagne, C., Magand, O., Martin, L., Mashyanov, N., Mkololo, T., Munthe, J., Obolkin, V., Ramirez Islas, M., Sena, F., Somerset, V., Spandow, P., Vardè, M., Walters, C., Wängberg, I., Weigelt, A., Yang, X., Zhang, H., 2017. Five-year records of mercury wet deposition flux at GMOS sites in the Northern and Southern hemispheres. *Atmos. Chem. Phys.* 17, 2689–2708. <https://doi.org/10.5194/acp-17-2689-2017>
- Sprovieri, F., Pirrone, N., Ebinghaus, R., Kock, H., Dommergue, A., 2010. A review of worldwide atmospheric mercury measurements. *Atmospheric Chemistry and Physics* 10, 8245–8265. <https://doi.org/10.5194/acp-10-8245-2010>
- Stager, J.C., Rvyes, D.B., Chase, B.M., Pausata, F.S.R., 2011. Catastrophic Drought in the Afro-Asian Monsoon Region During Heinrich Event 1. *Science* 331, 1299–1302. <https://doi.org/10.1126/science.1198322>
- Swart, P.K., 2015. The geochemistry of carbonate diagenesis: The past, present and future. *Sedimentology* 62, 1233–1304. <https://doi.org/10.1111/sed.12205>
- Talbot, M.R., Johannessen, T., 1992. A high resolution palaeoclimatic record for the last 27,500 years in tropical West Africa from the carbon and nitrogen isotopic composition of lacustrine organic matter. *Earth and Planetary Science Letters* 110, 23–37. [https://doi.org/10.1016/0012-821X\(92\)90036-U](https://doi.org/10.1016/0012-821X(92)90036-U)
- Them, T.R., Jagoe, C.H., Caruthers, A.H., Gill, B.C., Grasby, S.E., Gröcke, D.R., Yin, R., Owens, J.D., 2019. Terrestrial sources as the primary delivery mechanism of mercury to the oceans across the Toarcian Oceanic Anoxic Event (Early Jurassic). *Earth and Planetary Science Letters* 507, 62–72. <https://doi.org/10.1016/j.epsl.2018.11.029>
- Tisserand, D., Guédron, S., Viollier, E., Jézéquel, D., Rigaud, S., Campillo, S., Sarret, G., Charlet, L., Cossa, D., 2022. Mercury, organic matter, iron, and sulfur co-cycling in a ferruginous meromictic lake. *Applied Geochemistry* 146, 105463. <https://doi.org/10.1016/j.apgeochem.2022.105463>
- Tjallingii, R., Claussen, M., Stuut, J.-B.W., Fohlmeister, J., Jahn, A., Bickert, T., Lamy, F., Röhl, U., 2008. Coherent high- and low-latitude control of the northwest African hydrological balance. *Nature Geosci* 1, 670–675. <https://doi.org/10.1038/ngeo289>
- Trauth, M.H., Asrat, A., Berner, N., Bibi, F., Foerster, V., Grove, M., Kaboth-Bahr, S., Maslin, M.A., Mudelsee, M., Schäbitz, F., 2021. Northern Hemisphere Glaciation, African climate and human evolution. *Quaternary Science Reviews* 268, 107095. <https://doi.org/10.1016/j.quascirev.2021.107095>
- Tribouillard, N., Algeo, T.J., Lyons, T., Riboulleau, A., 2006. Trace metals as paleoredox and paleoproductivity proxies: An update. *Chemical Geology* 232, 12–32. <https://doi.org/10.1016/j.chemgeo.2006.02.012>
- Turner, B.F., Gardner, L.R., Sharp, W.E., 1996. The hydrology of lake Bosumtwi, a climate-sensitive lake in Ghana, West Africa. *Journal of Hydrology* 183, 243–261. [https://doi.org/10.1016/0022-1694\(95\)02982-6](https://doi.org/10.1016/0022-1694(95)02982-6)
- United Nations Environment Programme, 2018. Global Mercury Assessment, United Nations.
- Vindušková, O., Jandová, K., Frouz, J., 2019. Improved method for removing siderite by *in situ* acidification before elemental and isotope analysis of soil organic carbon. *J. Plant Nutr. Soil Sci.* 182, 82–91. <https://doi.org/10.1002/jpln.201800164>
- Vinnepand, M., Zeeden, C., Wonik, T., Gosling, W., Noren, A., Kück, J., Pierdominici, S., Voigt, S., Abadi, M.S., Ulfers, A., Danour, S., Afrifa, K., Kaboth-Bahr, S., 2024. An age-depth model for Lake Bosumtwi (Ghana) to reconstruct one million years of West African climate and environmental change. *Quaternary Science Reviews* 325, 108478. <https://doi.org/10.1016/j.quascirev.2023.108478>
- Weldeab, S., Lea, D.W., Schneider, R.R., Andersen, N., 2007. 155,000 Years of West African Monsoon and Ocean Thermal Evolution. *Science* 316, 1303–1307. <https://doi.org/10.1126/science.1140461>
- White, F. (Frank), 1983. The vegetation of Africa: a descriptive memoir to accompany the Unesco/AETFAT/UNSO vegetation map of Africa, Natural resources research ; 20. Unesco, Paris.
- Woolway, R.I., Kraemer, B.M., Lenters, J.D., Merchant, C.J., O'Reilly, C.M., Sharma, S., 2020. Global lake responses to climate change. *Nature Reviews Earth and Environment* 1, 388–403. <https://doi.org/10.1038/s43017-020-0067-5>
- Yin, R., Wang, X., Sun, R., Gao, L., Deng, C., Tian, Z., Luo, A., Lehmann, B., 2024. Linking the mercury biogeochemical cycle to the deep mercury cycle: A mercury isotope perspective. *Chemical Geology* 654, 122063. <https://doi.org/10.1016/j.chemgeo.2024.122063>
- Zaferani, S., Biester, H., 2021. Mercury Accumulation in Marine Sediments – A Comparison of an Upwelling Area and Two Large River Mouths. *Front. Mar. Sci.* 8, 732720. <https://doi.org/10.3389/fmars.2021.732720>
- Zolitschka, B., Francus, P., Ojala, A.E.K., Schimmelmänn, A., 2015. Varves in lake sediments - a review. *Quaternary Science Reviews* 117, 1–41.
- Zou, J., Chang, Y.P., Zhu, A., Chen, M.T., Kandasamy, S., Yang, H., Cui, J., Yu, P.S., Shi, X., 2021. Sedimentary mercury and antimony revealed orbital-scale dynamics of the Kuroshio Current. *Quaternary Science Reviews* 265, 107051. <https://doi.org/10.1016/j.quascirev.2021.107051>
- Åkerblom, S., Bishop, K., Björn, E., Lambertsson, L., Eriksson, T., Nilsson, M.B., 2013. Significant interaction effects from sulfate deposition and climate on sulfur concentrations constitute major controls on

1192 methylmercury production in peatlands. *Geochimica et Cosmochimica Acta* 102, 1–11.
1193 <https://doi.org/10.1016/j.gca.2012.10.025>

1194 Amos, H.M., Senke, J.E., Obrist, D., Robins, N., Hagan, N., Horowitz, H.M., Mason, R.P., Witt, M., Hodgecock,
1195 I.M., Corbitt, E.S., Sunderland, E.M., 2015. Observational and modeling constraints on global
1196 anthropogenic enrichment of mercury. *Environmental Science and Technology* 49, 4036–4047.
1197 <https://doi.org/10.1021/es5058665>

1198 Armenteros, I., 2010. Diagenesis of Carbonates in Continental Settings, in: *Developments in Sedimentology*.
1199 Elsevier, pp. 61–151. [https://doi.org/10.1016/S0070-4571\(09\)06202-5](https://doi.org/10.1016/S0070-4571(09)06202-5)

1200 Armstrong, E., Tallavaara, M., Hoperoff, P.O., Valdes, P.J., 2023. North African humid periods over the past
1201 800,000 years. *Nat Commun* 14, 5549. <https://doi.org/10.1038/s41467-023-41219-4>

1202 Benoit, J.M., Gilmour, C.C., Mason, R.P., Heyes, A., 1999. Sulfide controls on mercury speciation and
1203 bioavailability to methylating bacteria in sediment pore water. *Environmental Science and Technology*
1204 33, 1780. <https://doi.org/10.1021/es992007q>

1205 Biester, H., Pérez-Rodríguez, M., Giffedder, B.-S., Martínez Cortizas, A., Hermanns, Y.-M., 2018. Solar
1206 irradiance and primary productivity controlled mercury accumulation in sediments of a remote lake in the
1207 Southern Hemisphere during the past 4000 years: Primary productivity and mercury accumulation.
1208 *Limnol. Oceanogr.* 63, 540–549. <https://doi.org/10.1002/lno.10647>

1209 Bin, C., Xiaoru, W., Lee, F.S.C., 2001. Pyrolysis coupled with atomic absorption spectrometry for the
1210 determination of mercury in Chinese medicinal materials. *Analytica Chimica Acta* 447, 161–169.
1211 [https://doi.org/10.1016/S0003-2670\(01\)01218-4](https://doi.org/10.1016/S0003-2670(01)01218-4)

1212 Bishop, K., Shanley, J.B., Riscassi, A., de Wit, H.A., Eklöf, K., Meng, B., Mitchell, C., Osterwalder, S., Schuster,
1213 P.F., Webster, J., Zhu, W., 2020. Recent advances in understanding and measurement of mercury in
1214 the environment: Terrestrial Hg cycling. *Science of the Total Environment* 721.
1215 <https://doi.org/10.1016/j.scitotenv.2020.137647>

1216 Blais, J.M., Kalf, J., 1995. The influence of lake morphometry on sediment focusing. *Limnol. Oceanogr.* 40, 582–
1217 588. <https://doi.org/10.4319/lo.1995.40.3.0582>

1218 Boamah, D., Koeberl, C., 2007. The Lake Bosumtwi impact structure in Ghana: A brief environmental
1219 assessment and discussion of ecotourism potential. *Meteoritics and Planetary Science* 42, 561–567.
1220 <https://doi.org/10.1111/j.1945-5100.2007.tb01061.x>

1221 Bradley, R.S., Diaz, H.F., 2021. Late Quaternary Abrupt Climate Change in the Tropics and Sub-Tropics: The
1222 Continental Signal of Tropical Hydroclimatic Events (THEs). *Reviews of Geophysics* 59,
1223 e2020RG000732. <https://doi.org/10.1029/2020RG000732>

1224 Branfireun, B.A., Cosio, C., Poulain, A.J., Riise, G., Bravo, A.G., 2020. Mercury cycling in freshwater systems—
1225 An updated conceptual model. *Science of the Total Environment* 745.
1226 <https://doi.org/10.1016/j.scitotenv.2020.140906>

1227 Bravo, A.G., Bouchet, S., Tolu, J., Björn, E., Mateos-Rivera, A., Bortolsson, S., 2017. Molecular composition of
1228 organic matter controls methylmercury formation in boreal lakes. *Nat Commun* 8, 14255.
1229 <https://doi.org/10.1038/ncomms14255>

1230 Brodie, C.R., Leng, M.J., Casford, J.S.L., Kendrick, C.P., Lloyd, J.M., Yongqiang, Z., Bird, M.I., 2011. Evidence
1231 for bias in C and N concentrations and $\delta^{13}C$ composition of terrestrial and aquatic organic materials due
1232 to pre-analysis acid preparation methods. *Chemical Geology* 282, 67–83.
1233 <https://doi.org/10.1016/j.chemgeo.2011.01.007>

1234 Brooks, K., Scholz, C.A., King, J.W., Peck, J., Overpeck, J.T., Russell, J.M., Amoako, P.Y.O., 2005. Late-
1235 Quaternary lowstands of lake Bosumtwi, Ghana: Evidence from high-resolution seismic-reflection and
1236 sediment-core data. *Palaeogeography, Palaeoclimatology, Palaeoecology* 216, 235–249.
1237 <https://doi.org/10.1016/j.palaeo.2004.10.005>

1238 Brumsack, H.J., 2006. The trace metal content of recent organic carbon-rich sediments: Implications for
1239 Cretaceous black shale formation. *Palaeogeography, Palaeoclimatology, Palaeoecology* 232, 344–361.
1240 <https://doi.org/10.1016/j.palaeo.2005.05.014>

1241 Chang, M., Liu, B., Wang, B., Martinez-Villalobos, C., Ren, G., Zhou, T., 2022. Understanding Future Increases
1242 in Precipitation Extremes in Global Land Monsoon Regions. *Journal of Climate* 35, 1839–1851.
1243 <https://doi.org/10.1175/JCLI-D-21-0409.1>

1244 Chede, B.S., Venancio, I.M., Figueiredo, T.S., Albuquerque, A.L.S., Silva-Filho, E.V., 2022. Mercury deposition in
1245 the western tropical South Atlantic during the last 70 ka. *Palaeogeography, Palaeoclimatology,
1246 Palaeoecology* 601, 111122. <https://doi.org/10.1016/j.palaeo.2022.111122>

1247 Cohen, A., Campisano, C., Arrowsmith, R., Asrat, A., Behrensmeyer, A.K., Deino, A., Feibel, C., Hill, A.,
1248 Johnson, R., Kingston, J., Lamb, H., Lowenstein, T., Noren, A., Olago, D., Owen, R.B., Potts, R., Reed,
1249 K., Renaut, R., Schäbitz, F., Tiercelin, J.-J., Trauth, M.H., Wynn, J., Ivory, S., Brady, K., O'Grady, R.,
1250 Rodysill, J., Githiri, J., Russell, J., Foerster, V., Dommain, R., Rucina, S., Deocampo, D., Russell, J.,
1251 Billingsley, A., Beck, C., Dorenbek, G., Dullo, L., Feary, D., Garello, D., Gromig, R., Johnson, T.,
1252 Junginger, A., Karanja, M., Kimburi, E., Mbutia, A., McCartney, T., McNulty, E., Muiruri, V., Nambiro,
1253 E., Negash, E.W., Njagi, D., Wilson, J.N., Rabideaux, N., Raub, T., Sier, M.J., Smith, P., Urban, J.,
1254 Warren, M., Yadeta, M., Yost, C., Zinaye, B., 2016. The Hominin Sites and Paleolakes Drilling Project:
1255 inferring the environmental context of human evolution from eastern African rift lake deposits. *Scientific
1256 Drilling* 21, 1–16. <https://doi.org/10.5194/sd-21-1-2016>

1257 Cohen, A.S., Campisano, C.J., Arrowsmith, J.R., Asrat, A., Beck, C.C., Behrensmeyer, A.K., Deino, A.L., Feibel,
1258 C.S., Foerster, V., Kingston, J.D., Lamb, H.F., Lowenstein, T.K., Lupien, R.L., Muiruri, V., Olago, D.O.,

Formatted: German (Switzerland)

Owen, R.B., Potts, R., Russell, J.M., Schaebitz, F., Stone, J.R., Trauth, M.H., Yost, C.L., 2022. Reconstructing the Environmental Context of Human Origins in Eastern Africa Through Scientific Drilling. *Annu. Rev. Earth Planet. Sci.* 50, 451–476. <https://doi.org/10.1146/annurev-earth-031920-081947>

Cohen, A.S., Stone, J.R., Beuning, K.R.M., Park, L.E., Reinthal, P.N., Dettman, D., Scholz, C.A., Johnson, T.C., King, J.W., Talbot, M.R., Brown, E.T., Ivory, S.J., 2007. Ecological consequences of early Late Pleistocene megadroughts in tropical Africa. *PNAS U.S.A.* 104, 16422–16427. <https://doi.org/10.1073/pnas.0703873104>

Cooke, C.A., Martinez-Cortizas, A., Bindler, R., Sexauer Gustin, M., 2020. Environmental archives of atmospheric Hg deposition—A review. *Science of the Total Environment* 709, 134800. <https://doi.org/10.1016/j.scitotenv.2019.134800>

Deplazes, G., Lückge, A., Peterson, L.C., Timmermann, A., Hamann, Y., Hughen, K.A., Röhl, U., Laj, C., Cane, M.A., Sigman, D.M., Haug, G.H., 2013. Links between tropical rainfall and North Atlantic climate during the last glacial period. *Nature Geoscience* 6, 213–217. <https://doi.org/10.1038/ngeo1712>

Edwards, B.A., Kushner, D.S., Outridge, P.M., Wang, F., 2021. Fifty years of volcanic mercury emission research: Knowledge gaps and future directions. *Science of the Total Environment* 757, 143800. <https://doi.org/10.1016/j.scitotenv.2020.143800>

Engstrom, D.R., Rose, N.L., 2013. A whole-basin, mass-balance approach to paleolimnology. *J. Paleolimnol.* 49, 333–347. <https://doi.org/10.1007/s10933-012-9675-5>

Fadina, O.A., Venancio, I.M., Belem, A., Silveira, C.S., Bertagnolli, D. de C., Silva-Filho, E.V., Albuquerque, A.L.S., 2019. Paleoclimatic controls on mercury deposition in northeast Brazil since the Last Interglacial. *Quaternary Science Reviews* 221, 105869. <https://doi.org/10.1016/j.quascirev.2019.105869>

Figueiredo, T.S., Bergquist, B.A., Santos, T.P., Albuquerque, A.L.S., Silva-Filho, E.V., 2022. Relationship between glacial CO₂ drawdown and mercury cycling in the western South Atlantic: An isotopic insight. *Geology* 50, 3–7. <https://doi.org/10.1130/g49942.1>

Foerster, V., Asrat, A., Bronk Ramsey, C., Brown, E.T., Chapot, M.S., Deino, A., Duesing, W., Grove, M., Hahn, A., Junginger, A., Kaboth-Bahr, S., Lane, C.S., Opitz, S., Noren, A., Roberts, H.M., Stockhecke, M., Tiedemann, R., Vidal, C.M., Vogelsang, R., Cohen, A.S., Lamb, H.F., Schaebitz, F., Trauth, M.H., 2022. Pleistocene climate variability in eastern Africa influenced hominin evolution. *Nature Geoscience* 15, 805–811. <https://doi.org/10.1038/s41561-022-01032-y>

Francisco López, A., Heckenauer Barrón, E.G., Bello Bugallo, P.M., 2022. Contribution to understanding the influence of fires on the mercury cycle: Systematic review, dynamic modelling and application to sustainable hypothetical scenarios. *Environmental Monitoring & Assessment* 194, 707. <https://doi.org/10.1007/s10661-022-10208-3>

Frieling, J., Mather, T.A., März, C., Jenkyns, H.C., Hennekam, R., Reichert, G.-J., Slomp, C.P., Van Helmond, N.A.G.M., 2023. Effects of redox variability and early diagenesis on marine sedimentary Hg records. *Geochimica et Cosmochimica Acta* S0016703723001850. <https://doi.org/10.1016/j.gca.2023.04.015>

Gehrke, G.E., Blum, J.D., Meyers, P.A., 2009. The geochemical behavior and isotopic composition of Hg in a mid-Pleistocene western Mediterranean sapropel. *Geochimica et Cosmochimica Acta* 73, 1651–1665. <https://doi.org/10.1016/j.gca.2008.12.012>

Gosling, W.D., McMichael, C.N.H., Groenwoud, Z., Roding, E., Miller, C.S., Julier, A.C.M., 2021. Preliminary evidence for green, brown and black worlds in tropical western Africa during the Middle and Late Pleistocene. *Palaeogeography of Africa* 35, 13–25. <https://doi.org/10.1201/9781003162766>

Gosling, W.D., Miller, C.S., Shanahan, T.M., Holden, P.B., Overpeck, J.T., van Langevelde, Frank., 2022a. A stronger role for long-term moisture change than for CO₂ in determining tropical woody vegetation change. *Science* 376, 653–656. <https://doi.org/10.1126/science.abg4618>

Gosling, W.D., Scerri, E.M.L., Kaboth-Bahr, S., 2022b. The climate and vegetation backdrop to hominin evolution in Africa. *Philosophical Transactions of the Royal Society B: Biological Sciences* 377. <https://doi.org/10.1098/rstb.2020.0483>

Grant, K.M., Amarathunga, U., Amies, J.D., Hu, P., Qian, Y., Penny, T., Rodriguez-Sanz, L., Zhao, X., Heslop, D., Liebrand, D., Hennekam, R., Westerhold, T., Gilmore, S., Lourens, L.J., Roberts, A.P., Rohling, E.J., 2022. Organic carbon burial in Mediterranean sapropels intensified during Green Sahara Periods since 3.2 Myr ago. *Communications Earth & Environment* 3, 11. <https://doi.org/10.1038/s43247-021-00339-9>

Grant, K.M., Grimm, R., Mikolajewicz, U., Marino, G., Ziegler, M., Rohling, E.J., 2016. The timing of Mediterranean sapropel deposition relative to insolation, sea-level and African monsoon changes. *Quaternary Science Reviews* 140, 125–141. <https://doi.org/10.1016/j.quascirev.2016.03.026>

Grant, K.M., Rohling, E.J., Westerhold, T., Zabel, M., Heslop, D., Konijnendijk, T., Lourens, L., 2017. A 3 million year index for North African humidity/aridity and the implication of potential pan-African humid periods. *Quaternary Science Reviews* 171, 100–118. <https://doi.org/10.1016/j.quascirev.2017.07.005>

Grygar, T.M., Mach, K., Martinez, M., 2019. Checklist for the use of potassium concentrations in siliciclastic sediments as paleoenvironmental archives. *Sedimentary Geology* 382, 75–84. <https://doi.org/10.1016/j.sedgeo.2019.01.010>

Guédron, S., Ledru, M.P., Escobar-Torrez, K., Develle, A.L., Brisset, E., 2018. Enhanced mercury deposition by Amazonian orographic precipitation: Evidence from high-elevation Holocene records of the Lake Titicaca region (Bolivia). *Palaeogeography, Palaeoclimatology, Palaeoecology* 511, 577–587. <https://doi.org/10.1016/j.palaeo.2018.09.023>

1325 Gulati, R.D., Zadereev, E.S., Degermendzhi, A.G. (Eds.), 2017. Ecology of Meromictic Lakes, Ecological Studies.
 1326 Springer International Publishing, Cham. <https://doi.org/10.1007/978-3-319-49143-1>

1327 Gustin, M.S., Bank, M.S., Bishop, K., Bowman, K., Branfireun, B., Chétolat, J., Eckley, C.S., Hammerschmidt,
 1328 C.R., Lamberg, C., Lyman, S., Martinez-Cortizas, A., Sommar, J., Tsui, M.T.-K., Zhang, T., 2020.
 1329 Mercury biogeochemical cycling: A synthesis of recent scientific advances. *Science of The Total*
 1330 *Environment* 737, 139619. <https://doi.org/10.1016/j.scitotenv.2020.139619>

1331 Han, S., Obraztsova, A., Pretto, P., Deheyn, D.D., Gieskes, J., Tebo, B.M., 2008. Sulfide and iron control on
 1332 mercury speciation in anoxic estuarine sediment slurries. *Marine Chemistry* 111, 214–220.
 1333 <https://doi.org/10.1016/j.marchem.2008.05.002>

1334 Hermanns, Y.M., Biester, H., 2013. A 17,300-year record of mercury accumulation in a pristine lake in southern
 1335 Chile. *Journal of Paleolimnology* 49, 547–561. <https://doi.org/10.1007/s10933-012-9668-4>

1336 Hermanns, Y.M., Cortizas, A.M., Arz, H., Stein, R., Biester, H., 2013. Untangling the influence of in-lake
 1337 productivity and terrestrial organic matter flux on 4,250 years of mercury accumulation in Lake Hambro,
 1338 Southern Chile. *Journal of Paleolimnology* 49, 563–573. <https://doi.org/10.1007/s10933-012-9657-7>

1339 Hernández, A., Martín-Puertas, C., Moffa-Sánchez, P., Moreno-Chamarro, E., Ortega, P., Blockley, S., Cobb, K.,
 1340 Comas-Bru, L., Giralt, S., Goosse, H., Luterbacher, J., Martrat, B., Muscheler, R., Parnell, A., Pla-
 1341 Rabes, S., Sjöto, J., Scaife, A., Swingedouw, D., Wise, E., Xu, G., 2020. Modes of climate variability:
 1342 Synthesis and review of proxy-based reconstructions through the Holocene. *Earth-Science Reviews*
 1343 209, 103286. <https://doi.org/10.1016/j.earscirev.2020.103286>

1344 Hsu-Kim, H., Kucharzyk, K.H., Zhang, T., Deshusses, M.A., 2013. Mechanisms Regulating Mercury
 1345 Bioavailability for Methylating Microorganisms in the Aquatic Environment: A Critical Review.
 1346 *Environmental Science & Technology* 47, 2441–2456. <https://doi.org/10.1021/es304370g>

1347 Jenkyns, H.C., 1988. The Early Toarcian (Jurassic) Anoxic Event. *American Journal of Science*.
 1348 Jenkyns, H.C., Weedon, G.P., 2013. Chemostratigraphy (CaCO₃, TOC, δ¹³C_{org}) of Sinemurian (Lower Jurassic)
 1349 black shales from the Wessex Basin, Dorset and palaeoenvironmental implications. *Newsletters on*
 1350 *Stratigraphy* 46, 1–21. <https://doi.org/10.1127/0078-0421/2013/0029>

1351 Jeon, B., Scirio, A., Cizdziel, J.V., Chen, J., Black, O., Wallace, D.J., Zhou, Y., Lepak, R.F., Hurley, J.P., 2020.
 1352 Historical deposition of trace metals in a marine sapropel from Mangrove Lake, Bermuda with emphasis
 1353 on mercury, lead, and their isotopic composition. *Journal of Soils & Sediments* 20, 2266–2276.
 1354 <https://doi.org/10.1007/s11368-020-02567-6>

1355 Jourdan, F., Renne, P.R., Reimold, W.U., 2009. An appraisal of the ages of terrestrial impact structures. *Earth*
 1356 *and Planetary Science Letters* 286, 1–13. <https://doi.org/10.1016/j.epsl.2009.07.009>

1357 Kaboth-Bahr, S., Gosling, W.D., Vogelsang, R., Bahr, A., Scerri, E.M.L., 2021. Paleo-ENSO influence on African
 1358 environments and early modern humans. *PNAS* 118, 1–6. <https://doi.org/10.1073/pnas.2018277118>

1359 Kiely, R., 2023. A 50,000-year reconstruction of West African fire history (MSc Thesis). University of Amsterdam,
 1360 Amsterdam.

1361 Kinsley, C.W., Bradtmiller, L.I., McGee, D., Galgay, M., Stuut, J.B., Tjallingii, R., Winckler, G., DeMenocal, P.B.,
 1362 2022. Orbital and Millennial-Scale Variability in Northwest African Dust Emissions Over the Past 67,000
 1363 years. *Paleoceanography and Paleoclimatology* 37, 1–22. <https://doi.org/10.1029/2020PA004137>

1364 Koeberl, C., Milkereit, B., Overpeck, J.T., Scholz, C.A., Amoako, P.Y.O., Boamah, D., Danuor, S.K., Karp, T.,
 1365 Kueck, J., Hecky, R.E., King, J.W., Peack, J.A., 2007. An international and multidisciplinary drilling
 1366 project into a young complex impact structure: The 2004 ICDP Bosumtwi Crater Drilling Project—An
 1367 overview. *Meteoritics and Planetary Science* 42, 483–511. <https://doi.org/10.1111/j.1945-5100.2007.tb01057.x>

1368 Koeberl, C., Peck, J., King, J., Milkereit, B., Overpeck, J., Scholz, C., 2005. The ICDP lake Bosumtwi drilling
 1369 project: A first report. *Scientific Drilling* 1, 23–27. <https://doi.org/10.2204/iodp.sd.1.04.2005>

1370 Kuss, J., Zülke, C., Pohl, C., Schneider, B., 2011. Atlantic mercury emission determined from continuous
 1371 analysis of the elemental mercury sea-air concentration difference within transects between 50°N and
 1372 50°S. *Global Biogeochemical Cycles* 25. <https://doi.org/10.1029/2010GB003998>

1373 Larrasoana, J.C., Roberts, A.P., Rohling, E.J., 2013. Dynamics of Green Sahara Periods and Their Role in
 1374 Hominin Evolution. *PLoS ONE* 8. <https://doi.org/10.1371/journal.pone.0076514>

1375 Laskar, J., Robutel, P., Joutel, F., Gastineau, M., Correia, A.C.M., Levrard, B., 2004. A long-term numerical
 1376 solution for the insolation quantities of the Earth. *Astronomy and Astrophysics* 428, 261–285.
 1377 <https://doi.org/10.1051/0004-6361:20041335>

1378 Leiva-González, J., Díaz-Robles, L.A., Cereceda-Balic, F., Pino-Cortés, E., Campos, V., 2022. Atmospheric
 1379 Modelling of Mercury in the Southern Hemisphere and Future Research Needs: A Review. *Atmosphere*
 1380 13, 1226. <https://doi.org/10.3390/atmos13081226>

1381 Lent, R.M., Alexander, C.R., 1996. Mercury accumulation in Devils Lake, north Dakota – effects of environmental
 1382 variation in closed-basin lakes on mercury chronologies. *Water, Air, & Soil Pollution* 98, 275–296.

1383 Lézine, A.-M., Izumi, K., Kageyama, M., Achoundong, G., 2019. A 90,000-year record of Afromontane forest
 1384 responses to climate change. *Science* 363, 177–181. <https://doi.org/10.1126/science.aav6821>

1385 Li, F., Ma, C., Zhang, P., 2020. Mercury Deposition, Climate Change and Anthropogenic Activities: A Review.
 1386 *Frontiers in Earth Science* 8, 316. <https://doi.org/10.3389/feart.2020.00316>

1387 Lisiecki, L.E., Raymo, M.E., 2005. A Pliocene-Pleistocene stack of 57 globally distributed benthic δ-18O records.
 1388 *Paleoceanography* 20, 1–17. <https://doi.org/10.1029/2004PA001071>

Formatted: German (Switzerland)

Formatted: French (Switzerland)

Formatted: French (Switzerland)

Liu, M., Zhang, Q., Maavara, T., Liu, S., Wang, X., Raymond, P.A., 2021. Rivers as the largest source of mercury to coastal oceans worldwide. *Nature Geoscience* 14, 672–677. <https://doi.org/10.1038/s41561-021-00793-2>

Lyman, S.N., Cheng, I., Gratz, L.E., Weiss-Penzias, P., Zhang, L., 2020. An updated review of atmospheric mercury. *Science of the Total Environment* 707, 135675. <https://doi.org/10.1016/j.scitotenv.2019.135675>

Machado, W., Sanders, C.J., Santos, I.R., Sanders, L.M., Silva-Filho, E.V., Luiz-Silva, W., 2016. Mercury dilution by autochthonous organic matter in a fertilized mangrove wetland. *Environmental Pollution* 213, 30–35. <https://doi.org/10.1016/j.envpol.2016.02.002>

Mason, R.P., Laporte, J.M., Andres, S., 2000. Factors controlling the bioaccumulation of mercury, methylmercury, arsenic, selenium, and cadmium by freshwater invertebrates and fish. *Archives of Environmental Contamination and Toxicology* 38, 283–297. <https://doi.org/10.1007/s002449910038>

McKay, N.P., 2012. A multidisciplinary approach to late Quaternary paleoclimatology with an emphasis on sub-saharan West Africa and the last interglacial period (PhD Thesis). University of Arizona, Arizona.

Menviel, L., Govin, A., Avenas, A., Meissner, K.J., Grant, K.M., Tzedakis, P.C., 2021. Drivers of the evolution and amplitude of African Humid Periods. *Communications Earth & Environment* 2, 237. <https://doi.org/10.1038/s43247-021-00309-1>

Miller, C.S., Gosling, W.D., 2014. Quaternary forest associations in lowland tropical West Africa. *Quaternary Science Reviews* 84, 7–25. <https://doi.org/10.1016/j.quascirev.2013.10.027>

Miller, C.S., Gosling, W.D., Kemp, D.B., Coe, A.L., Gilmour, I., 2016. Drivers of ecosystem and climate change in tropical West Africa over the past ~540 000 years. *Journal of Quaternary Science* 31, 671–677. <https://doi.org/10.1002/jqs.2893>

Moore, H.R., Crocker, A.J., Bolcher, C.M., Meckler, A.N., Osborne, C.P., Beerling, D.J., Wilson, P.A., 2022. Hydroclimate variability was the main control on fire activity in northern Africa over the last 50,000 years. *Quaternary Science Reviews* 288, 107578. <https://doi.org/10.1016/j.quascirev.2022.107578>

Nalbant, J., Schneider, L., Hamilton, R., Connor, S., Biester, H., Stuart-Williams, H., Bergal-Kuvikas, O., Jacobsen, G., Stevenson, J., 2023. Fire, volcanism and climate change: the main factors controlling mercury (Hg) accumulation rates in Tropical Lake Lantoa, Sulawesi, Indonesia (~16,500–540 cal-yr BP). *Frontiers in Environmental Chemistry* 4, 1241176. <https://doi.org/10.3389/fenvc.2023.1241176>

Nicholson, S.E., 2013. The West African Sahel: A Review of Recent Studies on the Rainfall Regime and Its Interannual Variability. *JSRN Meteorology* 2013, 1–32. <https://doi.org/10.1155/2013/453521>

Obrist, D., Kirk, J.L., Zhang, L., Sunderland, E.M., Jiskra, M., Selin, N.E., 2018. A review of global environmental mercury processes in response to human and natural perturbations: Changes of emissions, climate, and land use. *Ambio* 47, 116–140. <https://doi.org/10.1007/s13280-017-1004-9>

Outridge, P.M., Stern, G.A., Hamilton, P.B., Sanei, H., 2019. Algal scavenging of mercury in preindustrial Arctic lakes. *Limnology & Oceanography* 64, 1558–1571. <https://doi.org/10.1002/lno.11135>

Outridge, Sanei, H., Stern, G.A., Goodarzi, F., 2007. Evidence for Control of Mercury Accumulation Rates in Canadian High Arctic Lake Sediments by Variations of Aquatic Primary Productivity. *Environmental Science & Technology* 41, 5259–5265. <https://doi.org/10.1021/es070408x>

Paine, A.R., Fendley, I.M., Frieling, J., Mather, T.A., Lacey, J.H., Wagner, B., Robinson, S.A., Pyle, D.M., Francke, A., Them II, T.R., Panagiotopoulos, K., 2024. Mercury records covering the past 90 000 years from lakes Prespa and Ohrid, SE Europe. *Biogeosciences* 21, 531–556. <https://doi.org/10.5194/bg-21-531-2024>

Pan, J., Zhong, W., Wei, Z., Ouyang, J., Shang, S., Ye, S., Chen, Y., Xue, J., Tang, X., 2020. A 15,400-year record of natural and anthropogenic input of mercury (Hg) in a sub-alpine lacustrine sediment succession from the western Nanling Mountains, South China. *Environmental Science and Pollution Research* 27, 20478–20489. <https://doi.org/10.1007/s11356-020-08421-z>

Pausata, F.S.R., Gaetani, M., Messori, G., Berg, A., Maia de Souza, D., Sage, R.F., deMenocal, P.B., 2020. The Greening of the Sahara: Past Changes and Future Implications. *One Earth* 2, 235–250. <https://doi.org/10.1016/j.oneear.2020.03.002>

Peck, J.A., Green, R.R., Shanahan, T., King, J.W., Overpeck, J.T., Scholz, C.A., 2004. A magnetic mineral record of Late Quaternary tropical climate variability from Lake Bosumtwi, Ghana. *Palaeogeography, Palaeoclimatology, Palaeoecology* 215, 37–57. <https://doi.org/10.1016/j.palaeo.2004.08.003>

Pérez-Rodríguez, M., Margalef, O., Corella, J.P., Saiz-Lopez, A., Pla-Rabes, S., Giralt, S., Cortizas, A.M., 2018. The role of climate: 71 ka of atmospheric mercury deposition in the southern hemisphere recorded by Rano Aroi Mire, Easter Island (Chile). *Geosciences (Switzerland)* 8. <https://doi.org/10.3390/geosciences8100374>

Pilla, R.M., Williamson, C.E., Adamovich, B.V., Adrian, R., Anneville, O., Chandra, S., Colom-Montero, W., Devlin, S.P., Dix, M.A., Dokulil, M.T., Gaiser, E.E., Girdner, S.F., Hambright, K.D., Hamilton, D.P., Havens, K., Hessen, D.O., Higgins, S.N., Huttula, T.H., Huuskonen, H., Isles, P.D.F., Joehnk, K.D., Jones, I.D., Keller, W.B., Knoll, L.B., Korhonen, J., Kraemer, B.M., Leavitt, P.R., Lepori, F., Luger, M.S., Maberly, S.C., Melack, J.M., Melles, S.J., Müller-Navarra, D.C., Pierson, D.C., Pislegina, H.V., Plisnier, P.-D., Richardson, D.C., Rimmer, A., Rogora, M., Rusak, J.A., Sadro, S., Salmasso, N., Saros, J.E., Saulnier-Talbot, E., Schindler, D.E., Schmid, M., Shimaraeva, S.V., Silow, E.A., Sitoki, L.M., Sommaruga, R., Straile, D., Strock, K.E., Thiery, W., Timofeyev, M.A., Verburg, P., Vinebrooke, R.D., Weyhenmeyer, G.A., Zadererev, E., 2020. Deeper waters are changing less consistently than surface waters in a global analysis of 102 lakes. *Scientific Reports* 10, 20514. <https://doi.org/10.1038/s41598-020-76873-x>

Formatted: French (Switzerland)

Formatted: German (Switzerland)

Formatted: French (Switzerland)

Pompeani, D.P., Cooke, C.A., Abbott, M.B., Drevnick, P.E., 2018. Climate, Fire, and Vegetation Mediate Mercury Delivery to Midlatitude Lakes over the Holocene. *Environmental Science and Technology* 52, 8157–8164. <https://doi.org/10.1021/acs.est.8b01623>

Ravichandran, M., 2004. Interactions between mercury and dissolved organic matter – A review. *Chemosphere* 55, 319–331. <https://doi.org/10.1016/j.chemosphere.2003.11.011>

Russell, J., Talbot, M.R., Haskell, B.J., 2003. Mid-holocene climate change in Lake Bosumtwi, Ghana. *Quaternary Research* 60, 133–141. [https://doi.org/10.1016/S0033-5894\(03\)00065-6](https://doi.org/10.1016/S0033-5894(03)00065-6)

Sanei, H., Grasby, S., Beauchamp, B., 2012. Latest Permian mercury anomalies. *Geology* 40, 63–66.

Schneider, L., Cooke, C.A., Stansell, N.D., Haberle, S.G., 2020. Effects of climate variability on mercury deposition during the Older Dryas and Younger Dryas in the Venezuelan Andes. *Journal of Paleolimnology* 63, 211–224. <https://doi.org/10.1007/s10933-020-00411-7>

Schneider, L., Fisher, J.A., Diéguez, M.C., Fostier, A.-H., Guimaraes, J.R.D., Leaner, J.J., Mason, R., 2023. A synthesis of mercury research in the Southern Hemisphere, part 1: Natural processes. *Ambio* 52, 897–917. <https://doi.org/10.1007/s13280-023-01832-5>

Scholz, C.A., Johnson, T.C., Cohen, A.S., King, J.W., Peck, J.A., Overpeck, J.T., Talbot, M.R., Brown, E.T., Kalindekale, L., Amoako, P.Y.O., Lyons, R.P., Shanahan, T.M., Castañeda, I.S., Heil, C.W., Forman, S.L., McHargue, L.R., Beuning, K.R., Gomez, J., Pierson, J., 2007. East African megadroughts between 135 and 75 thousand years ago and bearing on early modern human origins. *PNAS USA* 104, 16416–16421. <https://doi.org/10.1073/pnas.0703874104>

Schultze, M., Boehrer, B., Wendt-Potthoff, K., Katsev, S., Brown, E.T., 2017. Chemical Setting and Biogeochemical Reactions in Meromictic Lakes, in: *Ecology of Meromictic Lakes*, Springer, pp. 35–61.

Schütze, M., Gatz, P., Gilfedder, B., Biester, H., 2021. Why productive lakes are larger mercury sedimentary sinks than oligotrophic brown water lakes. *Limnology & Oceanography* 66, 1316–1332. <https://doi.org/10.1002/lno.11684>

Schütze, M., Tserendorj, G., Pérez-Rodríguez, M., Rösch, M., Biester, H., 2018. Prediction of Holocene mercury accumulation trends by combining palynological and geochemical records of lake sediments (Black Forest, Germany). *Geosciences (Switzerland)* 8. <https://doi.org/10.3390/geosciences8100358>

Sebag, D., Garcin, Y., Adatte, T., Deschamps, P., Ménot, G., Verrecchia, E.P., 2018. Correction for the siderite effect on Rock-Eval parameters: Application to the sediments of Lake Barombi (southwest Cameroon). *Organic Geochemistry* 123, 126–135. <https://doi.org/10.1016/j.orggeochem.2018.05.010>

Segato, D., Saiz-Lopez, A., Mahajan, A.S., Wang, F., Corella, J.P., Cuevas, C.A., Erhardt, T., Jensen, C.M., Zeppenfeld, C., Kjær, H.A., Turetta, C., Cairns, W.R.L., Barbante, C., Spolaor, A., 2023. Arctic mercury flux increased through the Last Glacial Termination with a warming climate. *Nature Geoscience* 16, 439–445. <https://doi.org/10.1038/s41561-023-01172-9>

Selin, N.E., 2009. Global biogeochemical cycling of mercury: a review. *Annual Review of Environmental Resources* 34, 43–63.

Shanahan, T.M., Beck, J.W., Overpeck, J.T., McKay, N.P., Pigati, J.S., Peck, J.A., Scholz, C.A., Heil, C.W., King, J., 2012. Late Quaternary sedimentological and climate changes at Lake Bosumtwi, Ghana: New constraints from laminae analysis and radiocarbon age modeling. *Palaeogeography, Palaeoclimatology, Palaeoecology* 361–362, 49–60. <https://doi.org/10.1016/j.palaeo.2012.08.001>

Shanahan, T.M., McKay, N.P., Hughen, K.A., Overpeck, J.T., Otto-Bliesner, B., Heil, C.W., King, J., Scholz, C.A., Peck, J., 2015. The time-transgressive termination of the African humid period. *Nature Geoscience* 8, 140–144. <https://doi.org/10.1038/ngeo2329>

Shanahan, T.M., Overpeck, J.T., Anchukaitis, K.J., Beck, J.W., Cole, J.E., Dettman, D.L., Peck, J.A., Scholz, C.A., King, J.W., 2009. Atlantic forcing of persistent drought in West Africa. *Science* 324, 377–380. <https://doi.org/10.1126/science.1166352>

Shanahan, T.M., Overpeck, J.T., Beck, J.W., Wheeler, C.W., Peck, J.A., King, J.W., Scholz, C.A., 2008a. The formation of biogeochemical laminations in Lake Bosumtwi, Ghana, and their usefulness as indicators of past environmental changes. *Journal of Paleolimnology* 40, 339–355. <https://doi.org/10.1007/s10933-007-9164-4>

Shanahan, T.M., Overpeck, J.T., Scholz, C.A., Beck, J.W., Peck, J., King, J.W., 2008b. Abrupt changes in the water balance of tropical West Africa during the late Quaternary. *Journal of Geophysical Research* 113, D42108. <https://doi.org/10.1029/2007JD009320>

Shanahan, T.M., Overpeck, J.T., Sharp, W.E., Scholz, C.A., Arko, J.A., 2007. Simulating the response of a closed-basin lake to recent climate changes in tropical West Africa (Lake Bosumtwi, Ghana). *Hydrological Processes* 21, 1678–1691. <https://doi.org/10.1002/hyp.6359>

Shanahan, T.M., Overpeck, J.T., Wheeler, C.W., Beck, J.W., Pigati, J.S., Talbot, M.R., Scholz, C.A., Peck, J., King, J.W., 2006. Paleoclimatic variations in West Africa from a record of late Pleistocene and Holocene lake level stands of Lake Bosumtwi, Ghana. *Palaeogeography, Palaeoclimatology, Palaeoecology* 242, 287–302. <https://doi.org/10.1016/j.palaeo.2006.06.007>

Shanahan, T.M., Peck, J.A., McKay, N., Heil, C.W., King, J., Forman, S.L., Hoffmann, D.L., Richards, D.A., Overpeck, J.T., Scholz, C., 2013. Age models for long lacustrine sediment records using multiple dating approaches – An example from Lake Bosumtwi, Ghana. *Quaternary Geochronology* 15, 47–60. <https://doi.org/10.1016/j.quageo.2012.12.001>

Shen, J., Feng, Q., Algeo, T.J., Liu, Jinling, Zhou, C., Wei, W., Liu, Jiangsi, Them, T.R., Gill, B.C., Chen, J., 2020. Sedimentary host phases of mercury (Hg) and implications for use of Hg as a volcanic proxy. *Earth and Planetary Science Letters* 543, 116333. <https://doi.org/10.1016/j.epsl.2020.116333>

Formatted: German (Switzerland)

Formatted: German (Switzerland)

Formatted: German (Switzerland)

Formatted: French (Switzerland)

Skonieczny, C., McGee, D., Winckler, G., Bory, A., Bradtmiller, L.I., Kinsley, C.W., Polissar, P.J., De Pol-Holz, R., Rossignol, L., Malaizé, B., 2019. Monsoon-driven Saharan dust variability over the past 240,000 years. *Science Advances* 5, 1–9. <https://doi.org/10.1126/sciadv.aav1887>

Soerensen, A.L., Mason, R.P., Balcom, P.H., Jacob, D.J., Zhang, Y., Kuss, J., Sunderland, E.M., 2014. Elemental Mercury Concentrations and Fluxes in the Tropical Atmosphere and Ocean. *Environmental Science & Technology* 48, 11312–11319. <https://doi.org/10.1021/es503109p>

Sprovieri, F., Pirrone, N., Bencardino, M., D'Amore, F., Angot, H., Barbante, C., Brunke, E.-G., Arcaga-Cabrera, F., Cairns, W., Comero, S., Diéguez, M. del C., Dommergue, A., Ebinghaus, R., Feng, X.B., Fu, X., Garcia, P.E., Gawlik, B.M., Hageström, U., Hansson, K., Horvat, M., Kotnik, J., Labuschagne, G., Magand, O., Martin, L., Mashyanov, N., Mkololo, T., Munthe, J., Obolkin, V., Ramirez Islas, M., Sena, F., Somerset, V., Spandow, P., Vardè, M., Walters, C., Wängberg, I., Weigelt, A., Yang, X., Zhang, H., 2017. Five-year records of mercury wet deposition flux at GMOS sites in the Northern and Southern hemispheres. *Atmospheric Chemistry & Physics* 17, 2689–2708. <https://doi.org/10.5194/acp-17-2689-2017>

Sprovieri, F., Pirrone, N., Ebinghaus, R., Kock, H., Dommergue, A., 2010. A review of worldwide atmospheric mercury measurements. *Atmospheric Chemistry and Physics* 10, 8245–8265. <https://doi.org/10.5194/acp-10-8245-2010>

Swart, P.K., 2015. The geochemistry of carbonate diagenesis: The past, present and future. *Sedimentology* 62, 1233–1304. <https://doi.org/10.1111/sed.12205>

Talbot, M.R., Johannessen, T., 1992. A high resolution palaeoclimatic record for the last 27,500 years in tropical West Africa from the carbon and nitrogen isotopic composition of lacustrine organic matter. *Earth and Planetary Science Letters* 110, 23–37. [https://doi.org/10.1016/0012-821X\(92\)90036-U](https://doi.org/10.1016/0012-821X(92)90036-U)

Them, T.R., Jagoe, C.H., Caruthers, A.H., Gill, B.C., Grasby, S.E., Gröcke, D.R., Yin, R., Owens, J.D., 2019. Terrestrial sources as the primary delivery mechanism of mercury to the oceans across the Toarcian Oceanic Anoxic Event (Early Jurassic). *Earth and Planetary Science Letters* 507, 62–72. <https://doi.org/10.1016/j.epsl.2018.11.029>

Tisserand, D., Guédron, S., Viollier, E., Jézéquel, D., Rigaud, S., Campillo, S., Sarret, G., Charlet, L., Cossa, D., 2022. Mercury, organic matter, iron, and sulfur co-cycling in a ferruginous meromictic lake. *Applied Geochemistry* 146, 105463. <https://doi.org/10.1016/j.apgeochem.2022.105463>

Tjallingii, R., Claussen, M., Stuut, J.-B.W., Fohlmeister, J., Jahn, A., Bickert, T., Lamy, F., Röhl, U., 2008. Coherent high- and low-latitude control of the northwest African hydrological balance. *Nature Geoscience* 1, 670–675. <https://doi.org/10.1038/ngeo289>

Trauth, M.H., Asrat, A., Berner, N., Bibi, F., Foerster, V., Grove, M., Kaboth-Bahr, S., Maslin, M.A., Mudelsee, M., Schäbitz, F., 2021. Northern Hemisphere Glaciation, African climate and human evolution. *Quaternary Science Reviews* 268, 107095. <https://doi.org/10.1016/j.quascirev.2021.107095>

Tribouillard, N., Algeo, T.J., Lyons, T., Riboulleau, A., 2006. Trace metals as paleoredox and paleoproductivity proxies: An update. *Chemical Geology* 232, 12–32. <https://doi.org/10.1016/j.chemgeo.2006.02.012>

Turner, B.F., Gardner, L.R., Sharp, W.E., 1996. The hydrology of lake Bosumtwi, a climate-sensitive lake in Ghana, West Africa. *Journal of Hydrology* 183, 243–261. [https://doi.org/10.1016/0022-1694\(95\)02982-6](https://doi.org/10.1016/0022-1694(95)02982-6)

United Nations Environment Programme, 2018. Global Mercury Assessment, United Nations.

Vindušková, O., Jandová, K., Frouz, J., 2019. Improved method for removing siderite by *in situ* acidification before elemental and isotope analysis of soil organic carbon. *Journal of Plant Nutrition and Soil Science* 182, 82–91. <https://doi.org/10.1002/jpln.201800164>

Weldeab, S., Lea, D.W., Schneider, R.R., Andersen, N., 2007. 155,000 Years of West African Monsoon and Ocean Thermal Evolution. *Science* 316, 1303–1307. <https://doi.org/10.1126/science.1140461>

White, F. (Frank), 1983. The vegetation of Africa: a descriptive memoir to accompany the Unesco/AETFAT/UNSO vegetation map of Africa, Natural resources research; 20. Unesco, Paris.

Woolway, R.I., Kraemer, B.M., Lenters, J.D., Merchant, C.J., O'Reilly, C.M., Sharma, S., 2020. Global lake responses to climate change. *Nature Reviews Earth and Environment* 1, 388–403. <https://doi.org/10.1038/s43017-020-0067-5>

Zaferani, S., Biester, H., 2021. Mercury Accumulation in Marine Sediments — A Comparison of an Upwelling Area and Two Large River Mouths. *Frontiers in Marine Science* 8, 732720. <https://doi.org/10.3389/fmars.2021.732720>

Zolitschka, B., Francus, P., Ojala, A.E.K., Schimmelmann, A., 2015. Varves in lake sediments — a review. *Quaternary Science Reviews* 117, 1–41.

Zou, J., Chang, Y.P., Zhu, A., Chen, M.T., Kandasamy, S., Yang, H., Cui, J., Yu, P.S., Shi, X., 2021. Sedimentary mercury and antimony revealed orbital-scale dynamics of the Kuroshio Current. *Quaternary Science Reviews* 265, 107051. <https://doi.org/10.1016/j.quascirev.2021.107051>

Formatted: French (Switzerland)

Formatted: German (Switzerland)

Formatted: German (Switzerland)